1-1-2014

Geochemical variations in the Quaternary Andean back-arc volcanism, southern Mendoza, Argentina

Venera Espanon
University of Wollongong, vre981@uowmail.edu.au

Allan Chivas
University of Wollongong, toschi@uow.edu.au

Leslie Kinsley
Australian National University, leslie.kinsley@anu.edu.au

Anthony Dosseto
University of Wollongong, tonyd@uow.edu.au

Geochemical variations in the Quaternary Andean back-arc volcanism, southern Mendoza, Argentina

Abstract

The Payenia Basaltic Province (PBP) is located 450 km east of the Chile-Peru trench in central west Argentina, behind the Andean arc front, constituting the back-arc. In order to evaluate the influence of the subducting slab as well as the magmatic source of this region, two volcanic fields located at comparable distance to the trench, having abundant basaltic products and similar eruptive timeframes were chosen. The Llancanelo (LLVF) and the Payún Matrú (PMVF) volcanic fields are part of the PBP and exhibit abundant basaltic activity during the Pleistocene. The geochemical data suggest that the LLVF has some arc signatures which have been described as weak as they are not as pronounced as in the Andean arc. The weak arc signature is not derived from slab dehydration as high Th enrichment relative to U cannot be explained by this process. We relate the Th enrichment as well as the lack of large residual garnet signatures, to slab sediments in the source. In the case of the PMVF, no arc signature has been inferred despite being only 30 km south of the LLVF. However the PMVF has a composition similar to that of the local intraplate end member, represented by the Rio Colorado volcanic field. The two volcanic fields, LLVF and PMVF, show indications of lower crustal assimilation as they trend towards the lower continental crust end member in Nb/U vs Ce/Pb and Nb/Yb vs Th/Yb diagrams. The geochemical differences between the LLVF and the PMVF as well as between several volcanic fields are illustrated using spatial distribution maps of geochemical ratios. Using this new approach, the decrease in arc signature can be traced in the back-arc and the higher enrichment in high field strength elements (HFSE) relative to large ion lithophile elements (LILE) in the PMVF compared to the LLVF is explicitly shown. These geospatial maps provide a graphical manner to illustrate the presence of two distinct types of volcanism (OIB-like and arc-like) occurring in the same Quaternary basaltic province.

Publication Details

Espanon, V. R., Chivas, A. R., Kinsley, L. P. J. & Dosseto, A. (2014). Geochemical variations in the Quaternary Andean back-arc volcanism, southern Mendoza, Argentina. Lithos, 208-209 251-264.

*Geochemical variations in the Quaternary Andean back-arc volcanism, southern Mendoza, Argentina**

Venera R. Espanon [a,b], Allan R. Chivas[a], Leslie P.J. Kinsley[c] and Anthony Dosseto[a,b]

[a] *GeoQuEST Research Centre, School of Earth & Environmental Sciences, University of Wollongong, NSW 2522, Australia.*

[b] *Wollongong Isotope Geochronology Laboratory, School of Earth & Environmental Sciences, University of Wollongong, NSW 2522, Australia*.

[c] *Research School of Earth Sciences, The Australian National University, Canberra, ACT 0200, Australia.*

Allan R. Chivas: toschi@uow.edu.au

Leslie J. Kinsley: leslie.kinsley@anu.edu.au

Anthony Dosseto: tonyd@uow.edu.au

*Manuscript published (2014) in *Lithos*, volume 208–209, pages 251-264
DOI:10.1016/j.lithos.2014.09.010

Abstract

The Payenia Basaltic Province (PBP) is located 450 km east of the Chile-Peru trench in central west Argentina, behind the Andean arc front, constituting the back-arc. In order to evaluate the influence of the subducting slab as well as the magmatic source of this region, two volcanic fields located at comparable distance to the trench, having abundant basaltic products and similar eruptive timeframes were chosen. The Llancanelo (LLVF) and the Payún Matrú (PMVF) volcanic fields are part of the Payenia Basaltic Province and exhibit abundant basaltic activity during the Pleistocene. The geochemical data suggest that the LLVF has some arc signatures which have been described as weak as they are not as pronounced as in the Andean arc. The weak arc signature is not derived from slab dehydration as high Th enrichment relative to U cannot be explained by this process. We relate the Th enrichment as well as the lack of large residual garnet signatures, to slab sediments in the source. In the case of the Payún Matrú volcanic field, no arc signature has been inferred despite being only 30 km south of the LLVF. However the PMVF has a composition similar to that of the local intraplate end-member, represented by the Río Colorado volcanic field. The two volcanic fields, LLVF and PMVF, show indications of lower crustal assimilation as they trend towards the lower continental crust end-member in Nb/U vs Ce/Pb and Nb/Yb vs Th/Yb diagrams.

The geochemical differences between the LLVF and the PMVF as well as between several volcanic fields are illustrated using spatial distribution maps of geochemical ratios. Using this new approach, the decrease in arc signature can be traced in the back- arc and the higher enrichment in high field strength elements (HFSE) relative to large ion lithophile elements (LILE) in the PMVF compared to the LLVF is explicitly shown. These geospatial maps provide a graphical manner to illustrate the presence of two distinct types of volcanism (OIB-like and arc-like) occurring in the same Quaternary basaltic province.

2.1. Introduction

The Patagonian basaltic provinces extend from 35° to 52°S and have been widely studied providing several explanations for occurrence of the continental back-arc volcanism. For instance, the back-arc volcanism of the late Oligocene to early Miocene Somuncura Plateau, part of the Patagonian Massif (PM, Figure 2.1), has been considered the result of asthenospheric upwelling (De Ignacio et al., 2001; Kay et al., 2007). In contrast, the late Miocene back-arc volcanism was associated with a period of shallow slab subduction in a compressional tectonic regime (Kay et al 2004; Kay et al., 2006 a, b; Kay and Copeland, 2006). In the same area, the angle of subduction increased during the Pliocene, producing extensional processes which facilitated the generation of the Quaternary basaltic volcanism present in the Payenia Basaltic Province (PBP, Figure 2.1; Kay et al., 2006a).

The basaltic melts erupted in the Payenia Basaltic Province continental back-arc are described as heterogeneous, as they have been variably influenced by slab components, lower crustal contamination and intraplate melts, associated with an ocean island basalt (OIB)-like mantle source (Germa et al., 2010; Hernando et al., 2012; Jacques et al., 2013; Kay et al., 2004; Søager et al., 2013; Søager and Holm, 2013). In the northern part of the PBP, the basalts have been associated with mixing between a south Atlantic MORB-like source and slab components (Jacques et al., 2013, Søager et al., 2013). The southern PBP presents geochemical signatures related to mantle upwelling and an OIB-like source with little or no influence from the subduction zone to the west, as best exemplified by the basalts from the Río Colorado volcanic field (Jacques et al., 2013; Kay et al 2004; Søager et al., 2013; Søager and Holm, 2013). The PBP has been the focus of several geochemical investigations (Bermudez and Delpino, 1989; Bertotto et al., 2009; Germa et al., 2010; Hernando et al., 2012; Paquaré et al., 2008; Søager et al., 2013) as it provides an optimum framework to investigate the magmatic processes related to a continental back-arc setting. Accordingly, the purpose of this investigation is (i) to determine the contribution of arc-type magmatism in the continental back-arc, (ii) to understand the spatial geochemical variation in this area and (iii) to describe and comprehend the processes responsible for the geochemical characteristics observed in the continental back-arc.

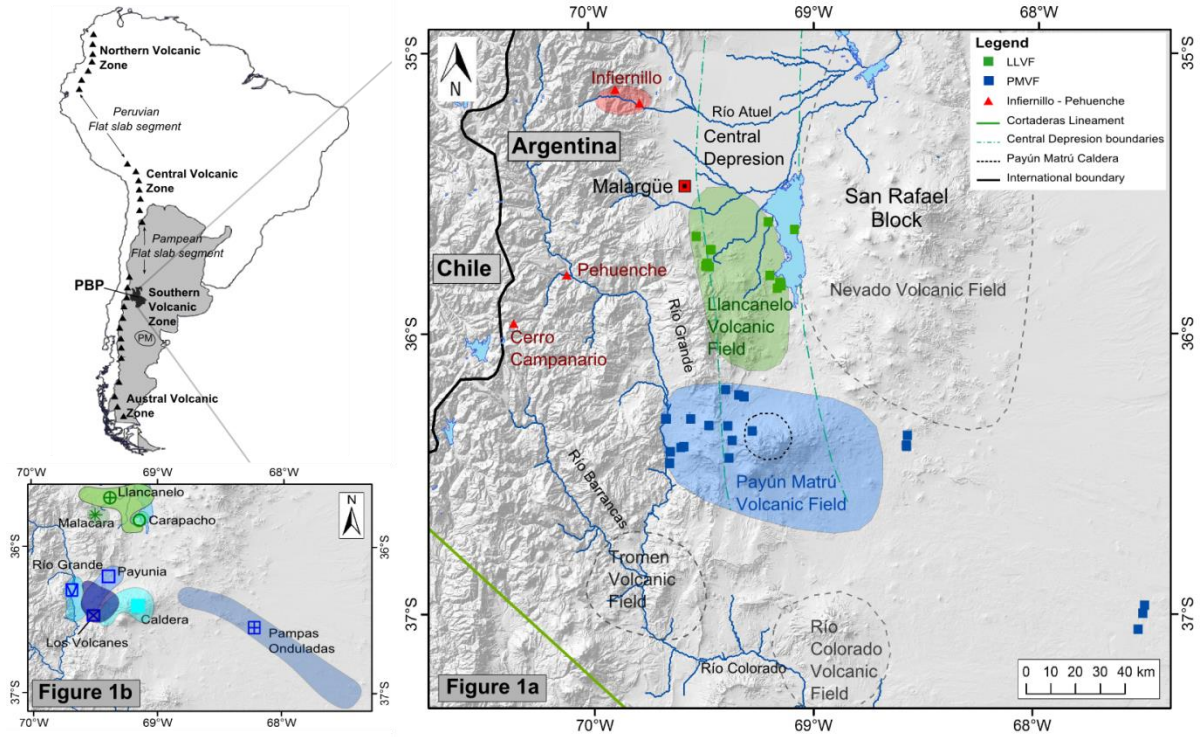

Figure 2.1. Geographical setting of the Payenia Basaltic Province (PBP). PM represents the Patagonian Massif. Figure 2.1a shows the geographic location of the volcanic fields. Green and blue fields represent the volcanic fields here investigated, while other volcanic fields are outlined in grey dashed lines. The green field is the Llancanelo volcanic field (LLVF) and the blue field is the Payún Matrú volcanic field (PMVF). Note that the blue squares located outside the PMVF correspond to Pampas Onduladas, a long flow (<160 km) that has its effusion point within the PMVF. The red field corresponds to the Infiernillo volcanic field. Red triangles correspond to felsic samples from Cerro Campanario and Pehuenche. The green dashed-point lines indicate the east and west boundaries of the Central Depression. The dashed circle delimits the Payún Matrú caldera. The black line indicates the international boundary and the green line indicates the Cortaderas lineament. Figure 2.1b shows the groups in which the Llancanelo volcanic field and the PMVF have been divided, with the corresponding symbol used in the following diagrams.

2.2. Geological Setting

Volcanism in the Andes extends from Colombia to the southern tip of South America and is related to the subduction of the Nazca Plate (from ~7.3°N to 45.6°S) and the Antarctic Plate (south of ~45.6°S) under the South American Plate. The Nazca Plate subducts beneath the Nazca Plate at an angle of 25 – 35°. Most volcanic activity in South America is restricted to the Andean volcanic arc, with the dominant volcanic product being intermediate to silicic (mainly andesite) and large amounts of pyroclastic material while areas of continental back-arc volcanism are evident to the east of the Andean volcanic arc.

The study area is located between 35°S and 37°S and 67°W and 70°W, in central-west Argentina (Figure 2.1) and is part of the northernmost Patagonian basaltic province named Payenia (Polanski, 1954; also called the Andino-Cuyana Basaltic Province by Bermudez and

Delpino, 1989). The Payenia Basaltic Province (PBP) was initially divided into the Llancanelo volcanic field to the north and the Payún Matrú volcanic field to the south (Bermudez and Delpino, 1989). Recently this initial division was reviewed by Gudnason et al. (2012) who redefined the original Llancanelo volcanic field from Bermudez and Delpino, (1989) into the Llancanelo and Nevado volcanic fields while the Payún Matrú volcanic field was divided into the Payún Matrú and Río Colorado volcanic fields (Figure 2.1a). The PBP encompasses an area of 15,900 km2 with more than 800 volcanic cones. This basaltic province is bounded on its western side by the Malargüe Fault and thrust belt, the central part is defined by a tectonic depression named the Central Depression (Llambías et al., 2010) and the eastern part is positioned on the uplifted San Rafael Block (Figure 2.1). The Central Depression was formed in the late Miocene during a period of shallow subduction that lasted until the early Quaternary in the northern PBP. North of 36°S, the Central Depression has been filled by approximately 1000 m of Cenozoic sediments (Ostera and Dalpeña, 2003) while south of 36°S, Cenozoic sedimentation was almost absent. Mesozoic sedimentary rocks of the Neuquén Basin underlie the sediments of the Central Depression. The southern limit of the Central Depression is not well defined as it vanishes south of the Payún Matrú caldera (Llambías et al., 2010).

The southern limit of the PBP is marked by the Cortaderas lineament (Ramos, 1978) south of which there is an absence of Cenozoic back-arc volcanism (Llambías et al., 2010). Volcanic activity has been evident in this continental back-arc since the earliest Miocene (Dyhr et al., 2013a; Gudnanson, et al., 2012; Kay and Coperland, 2006, Kay et al., 2006a; Kay et al., 2006b). However, Holocene volcanic activity is only known from the Payún Matrú volcanic field (Espanon et al., 2014a; Germa et al., 2010; Marchetti et al., 2014).

The current study is focused on the central part of the PBP, the Llancanelo volcanic field and the Payún Matrú volcanic field with the addition of some Andean arc samples from the areas of Cerro Campanario-Pehuenche and some retroarc samples from Infiernillo (Figure 2.1). Alkaline basalts are the dominant lithology in the PBP with minor silicic flows around the Payún Matrú caldera and the Cerro Nevado volcano (Llambías et al., 2010). The Llancanelo volcanic field has high cone density dominated by monogenetic scoria cones with some tuff rings (Risso et al., 2008). The two distinct phreatomagmatic volcanoes in this volcanic field are Carapacho and Malacara. Within the Llancanelo volcanic field, the volcanic cones are oriented along ENE-WSW trending fissures (Risso et al., 2008). The chronology of the Llancanelo volcanic field is not well constrained, however recent $^{40}Ar/^{39}Ar$ determinations suggest that it was active 1.1 Ma ago (Dyhr et al., 2013a) and the volcanic activity probably lasted until the late Pleistocene (Espanon et al., 2014a).

Most of the volcanism in the Payún Matrú volcanic field is monogenetic with only two polygenetic centres corresponding to the Payún Matrú caldera and the Payún Liso stratovolcano. The Payún Matrú caldera-forming event occurred approximately between 168 ka and 82 ka (Germa, et al., 2010), accompanied by an ignimbrite eruption which covered a vast

area up to 40 km (Hernando et al., 2012) from the caldera. This volcanic field has more than 220 scoria cones (Hernando et al., 2014b), many aligned along a major east-west fissure called La Carbonilla which is only exposed on the eastern side of the Payún Matrú caldera. The oldest part of this volcanic field is located on the eastern side of the Payún Matrú caldera and is also where the longest Quaternary basaltic flow is found, Pampas Onduladas (Pasquaré et al., 2008). The Payún Matrú volcanic field has been active during much of the Quaternary with some flows being less than 2 ka old (Marchetti et al., 2014).

The two volcanic fields investigated, Llancanelo and Payún Matrú volcanic fields are here sub-divided in order to assess their diversity. The criteria used to divide the volcanic fields are based on geographic and geochemical characteristics. The samples from Llancanelo volcanic field were divided into the Carapacho, Malacara and Llancanelo groups (Table 2.1). The Carapacho volcano resulted from explosive eruptions with direct magma-groundwater interaction. This volcano is characterised by abundant accidental lithic fragments (Llambías et al., 2010) and is therefore associated with a deeper water-magma interaction. The Malacara volcano has well defined basaltic flows to the north and it is composed of abundant scoria deposits with interbedded basaltic bombs. This volcano is a tuff cone and it was formed by dry and wet tephra fallout (Risso et al., 2008). It does not contain many accidental lithic fragments and is therefore considered to have formed by explosions close to the surface from an open vent. These two phreatomagmatic volcanoes have been analysed separately (Carapacho and Malacara groups), based on their geographical location and their distinct erupted products associated with differences in water-magma interaction. The remaining samples from the Llancanelo volcanic field that do not contain phreatomagmatic components have been placed in one group here designated the Llancanelo group.

The Payún Matrú volcanic field was divided into Los Volcanes, Río Grande, Payunia, Pampas Onduladas and Caldera groups. Los Volcanes group corresponds to young samples (~<10 ka, Espanon et al., 2014a; Marchetti et al., 2014) on the western side of the Payún Matrú caldera. This group is dominated by scoria cones and basaltic flows with a`a texture. The Río Grande group is characterised by pahoehoe basaltic flows that flow towards the Río Grande and are older than 10 ka (Germa et al., 2010; Marchetti et al., 2014). The Payunia group is composed of the remaining samples from the north-western side of the Payún Matrú caldera. The Pampas Onduladas group constitutes the basaltic samples from a compound long pahoehoe flow on the eastern side of the caldera and younger than 400 ka (Melchor and Casadio 1999; Pasquarè et al., 2008). The Caldera group, within the Payún Matrú volcanic field, is the only silicic group analysed from the continental back-arc and it includes samples from the Payún Matrú caldera.

2.3. Methods

Whole-rock samples were washed, dried and crushed in a Cr-Ni TEMA ring grinder (hence those elements were not used for the geochemical analysis). Samples with secondary mineralisation (SM16, VRE21, VRE46a, CP4, VRE27, VRE11 and VRE43) were soaked in 10% HCl for several hours to remove carbonate-filled vesicles followed by washing and drying prior to crushing. The leaching of these samples does not show a systematic shift with the samples that were not leached; nevertheless, trace-element duplicates were done for each of the leached samples using X-ray fluorescence analysis (Supplementary Table 2.1). The major-element analysis was by X-ray fluorescence on glass discs using a Spectro Xepos energy-dispersive polarisation X-ray spectrometer at the School of Earth and Environmental Sciences, University of Wollongong (Supplementary Table 2.1). Glass discs for the mafic samples were prepared by fusion of ~0.4g of ground sample and ~2.4 g of flux, which is a mixture of lithium tetraborate (35.3%), and lithium metaborate (64.7%). For the silicic samples, the flux used was 100% lithium metaborate. W-2 dolerite standard (n=4), was used during the period from October 2012 to November 2013 with a relative percentage standard deviation of <3 % for all the major elements.

Loss on ignition was measured using ~1 g of ground sample in a furnace at 1050°C. The glass discs prepared for major-element analysis were also analysed for 36 trace elements by LA-ICP-MS (Agilent 7200) at the Research School of Earth Sciences, Australian National University. The laser used was an Excimer laser (ArF 193 nm) 50 mJ, 5 Hz at a scan rate of 10 µm per second and a spot diameter of 105 µm. The data were calibrated using the international standard NIST612 (GEoReM reference material, Jochum et al., 2011) which was analysed under the same conditions as the samples. Reproducibility was monitored using the international rock standard BCR-2 (n=12) (USGS rock standard, Wilson, 1997) treated as an unknown and analysed under the same conditions as the samples. The relative standard deviation of BCR-2 ranges from 1.6 % to 5.7 % (2σ) for all elements (Supplementary Table 2.2). The major- and trace-element data obtained were plotted using the GeoChemical Data toolkit (GCDkit) developed by Janoušek et al. (2006).

Sr isotopic analysis was conducted on 9 samples (Table 2.2). Approximately 0.1 g of powdered sample was dissolved (only samples SM16 and VRE27 were previously leached with 10% HCl) in 1.5 mL 30% HCl, 2mL 70% $HClO_4$, 0.5 mL 65% HNO_3 and 2 mL 48% HF, at 130ºC for 12 hours. The samples were dried, re-dissolved in 2M HNO3 then loaded on a cation exchange column packed first with 0.1 mL Eichrom pre-filter® resin overlain by 0.2 mL Eichrom Sr-spec® resin (Moffat, 2013). Sr was eluted in 0.02M HNO_3 (Moffat, 2013). Sample preparation was performed in the Wollongong Isotope Geochronology Laboratory at the University of Wollongong while the Sr isotopic analysis was conducted using a Thermo Scientific Neptune multi-collector ICP-MS at the Research School of Earth Sciences, Australian National University. The precision of the Sr isotopic measurements was monitored by the SRM987

standard. The $^{87}Sr/^{86}Sr$ value obtained for SRM987 is 0.710342 ± 0.000007 (2σ) which is within the recommended value ($^{87}Sr/^{86}Sr$ = 0.71034 ± 0.00026, National institute of Standards and Technology, standard reference material 987). Total procedural blank for Sr is 52.4 pg which represents <0.003% of the total Sr analysed and was measured on an Agilent 7500cs quadrupole ICP-MS, at the School of Earth and Environmental Sciences, University of Wollongong.

Trace-element data (this study; Bertotto et al., 2009; Germa et al., 2010; Jacques et al., 2013; Pasquarè et al., 2008; Søager et al., 2013) were used to create several spatial distribution geochemical maps. The data from the current investigation and from previous publications were carefully examined and only samples with less than 53% SiO_2 were considered, in order to avoid geochemical modification of parent magma, by fractional crystallisation. A total of 255 and 230 data points were used and converted to a shapefile using the natural neighbourhood interpolation tool from ArcMap 10®. This tool was selected as it is the most appropriate method where sample data points are distributed with uneven density. Geospatial distribution maps were made at a broader scale (with 230 to 255 data points) including the back-arc fields and the Andean arc as well as on a more detailed scale (with ~112 data points) including the Llancanelo and the Payún Matrú volcanic field.

2.4. Results

2.4.1. Mineralogy

The basaltic rocks analysed have mainly a porphyritic texture, while some samples exhibit a glomeroporphyritic texture. The most abundant phenocrysts are olivine and plagioclase, with scarce pyroxene, opaque minerals and interstitial glass. The basaltic groundmass is composed of plagioclase and olivine with scattered pyroxene microcrysts. The olivine phenocrysts have a euhedral to subhedral shape, with some showing alteration to iddingsite especially for the samples from the Pampas Onduladas group. Opaque mineral phenocrysts were observed in most of the basalts. Euhedral plagioclase phenocrysts are abundant and are also the main component of crystal clots. The compositional zoning in plagioclase is normal with rare oscillatory zoning. The silicic samples from Payún Matrú caldera (here termed Caldera group) have been petrographically described by Germa et al. (2010) and Hernando et al. (2012). The Caldera group samples, have a porphyritic texture with abundant sanidine phenocrysts. The Infiernillo and Cerro Campanario-Pehuenche group samples have a glomeroporphyritic texture and are rich in feldspar phenocrysts.

Table 2.1. List of samples analysed including their area of origin and the group classification for each volcanic field. PMVF is the Payún Matrú volcanic field and LLVF is the Llancanelo volcanic field.

Area	Group classification	Sample	sample location	Latitude	Longitude	Material
PMVF	Los Volcanes	LV1	Los Volcanes	-36.33761	-69.47198	Basalt
PMVF	Los Volcanes	LV3	Los Volcanes	-36.31385	-69.55395	Basalt
PMVF	Los Volcanes	LV6	Los Volcanes	-36.45405	-69.38122	Basalt
PMVF	Los Volcanes	LV8	Los Volcanes	-36.41360	-69.58483	Basalt
PMVF	Los Volcanes	PN1	Pampas Negras	-36.39170	-69.36699	Basalt
PMVF	Río Grande	RG1	Río Grande	-36.47188	-69.64996	Basalt
PMVF	Río Grande	RG2	Río Grande	-36.47218	-69.65015	Basalt
PMVF	Río Grande	RG5	Río Grande	-36.31321	-69.66588	Basalt
PMVF	Río Grande	RG11	Río Grande	-36.43145	-69.64609	Basalt
PMVF	Río Grande	LV9	Los Volcanes	-36.41650	-69.59911	Basalt
PMVF	Río Grande	VRE12	La pasarela	-36.31422	-69.66344	Basalt
PMVF	Río Grande	VRE13	La pasarela	-36.31269	-69.66558	Basalt
PMVF	Payunia	VRE37	Payunia	-36.35861	-69.27650	Basalt
PMVF	Payunia	VRE38	Payunia	-36.33972	-69.38658	Basalt
PMVF	Payunia	VRE40	Payunia	-36.21031	-69.39516	Basalt
PMVF	Payunia	SM16	W side of Santa Maria	-36.22966	-69.33609	Basalt
PMVF	Payunia	SM17	W side of Santa Maria	-36.23573	-69.31216	Basalt
PMVF	Payunia	SM18	W side of Santa Maria	-36.23532	-69.31325	Basalt
PMVF	Pampas Onduladas	VRE19	Pampas Onduladas	-36.41244	-68.57889	Basalt
PMVF	Pampas Onduladas	VRE20	Pampas Onduladas	-36.40847	-68.58000	Basalt
PMVF	Pampas Onduladas	VRE21	Pampas Onduladas	-36.37317	-68.57544	Basalt
PMVF	Pampas Onduladas	VRE46 (A)	Pampas Onduladas	-36.97117	-67.49233	Basalt
PMVF	Pampas Onduladas	VRE47	Pampas Onduladas	-36.99872	-67.49917	Basalt
PMVF	Pampas Onduladas	VRE49	Pampas Onduladas	-37.05717	-67.52031	Basalt
PMVF	Caldera	VRE31	Payún Matrú	-36.37697	-69.25739	Trachytes
PMVF	Caldera	VRE33	Payún Matrú	-36.37667	-69.25872	Trachytes
PMVF	Caldera	VRE34	Payún Matrú	-36.37664	-69.25908	Trachytes
PMVF	Caldera	VRE35	Payún Matrú	-36.37672	-69.26119	Trachytes
PMVF	Caldera	VRE36	Payún Matrú	-36.35665	-69.27699	Trachytes

Table 1 (cont)

Area	Group classification	Sample	sample location	Latitude	Longitude	Material
PMVF	Caldera	VRE39	Payún Matrú	-36.25514	-69.40653	Trachytes
PMVF	Caldera	LV5	Los volcanes	-36.49188	-69.36781	Ignimbrite
PMVF	Caldera	LC1	La Calle	-36.45584	-69.38641	Ignimbrite
PMVF	Caldera	LC2	La Calle	-36.45621	-69.38509	Ignimbrite
LLVF	Carapacho	VRE25	Carapacho	-35.83594	-69.14550	Basalt
LLVF	Carapacho	VRE26 (A)	Carapacho	-35.83972	-69.14394	Basalt
LLVF	Carapacho	CP1	Carapacho	-35.82869	-69.15128	Tuff
LLVF	Carapacho	CP3	Carapacho	-35.82869	-69.15128	Basalt
LLVF	Carapacho	CP4	Carapacho	-35.82869	-69.15128	Tuff
LLVF	Malacara	VRE9	Malacara	-35.77222	-69.46592	Basalt
LLVF	Malacara	MC3	Malacara	-35.76870	-69.48225	Basalt
LLVF	Malacara	MC5	Malacara	-35.75967	-69.47816	Basalt
LLVF	Malacara	MC6	Malacara	-35.76090	-69.47373	Basalt
LLVF	Malacara	VRE27	Llancanelo	-35.71181	-69.45694	Basalt
LLVF	Llancanelo	VRE8	Llancanelo	-35.61292	-69.20192	Basalt
LLVF	Llancanelo	VRE11	Llancanelo	-35.63997	-69.08389	Basalt
LLVF	Llancanelo	VRE42	Llancanelo	-35.84869	-69.16200	Basalt
LLVF	Llancanelo	VRE43	Llancanelo	-35.80328	-69.19545	Basalt
LLVF	Llancanelo	VRE44	Llancanelo	-35.71044	-69.46106	Basalt
LLVF	Llancanelo	VRE45	Llancanelo	-35.66356	-69.52397	Basalt
retroarc	Infiernillo	VRE1	Infiernillo	-35.18650	-69.77327	basaltic-andesite
retroarc	Infiernillo	VRE4	Infiernillo	-35.13675	-69.88212	basaltic-andesite
retroarc	Infiernillo	VRE6	Infiernillo	-35.13689	-69.88161	basaltic-andesite
arc	Cerro Campanario-Pehuenche	VRE16A	Pehuenche	-35.79714	-70.10533	Rhyolite
arc	Cerro Campanario-Pehuenche	VRE16B	Pehuenche	-35.79714	-70.10533	Ignimbrite
arc	Cerro Campanario-Pehuenche	VRE17	Cerro Campanario	-35.96706	-70.34622	basaltic-andesite

2.4.2. Geochemistry

2.4.2.1. Major elements

The total alkali vs SiO_2 content diagram (Figure 2.2; Le Bas et al., 1986) shows that most samples from Llancanelo and Payún Matrú volcanic fields are alkaline basalts with the exception of samples from the caldera group which are silicic (trachytes and trachydacites). Samples from the Infiernillo group are basaltic andesites and have a composition similar to the Andean volcanic arc (Figures 2.2 and 2.3). The basalts from the Llancanelo and the Payún Matrú volcanic fields show similar variations among major-element oxide concentrations, while the Payún Matrú volcanic field basalts have higher TiO_2 and K_2O at a given MgO content than the Llancanelo volcanic field (Figure 2.3). The Caldera and Cerro Campanario-Pehuenche groups show very low MgO, TiO_2, CaO, P_2O_5, FeO_t and high SiO_2, Na_2O, K_2O contents (Figure 2.3) typical of their silicic nature. Infiernillo samples show an intermediate composition between the basalts and the silicic groups (Figure 2.3).

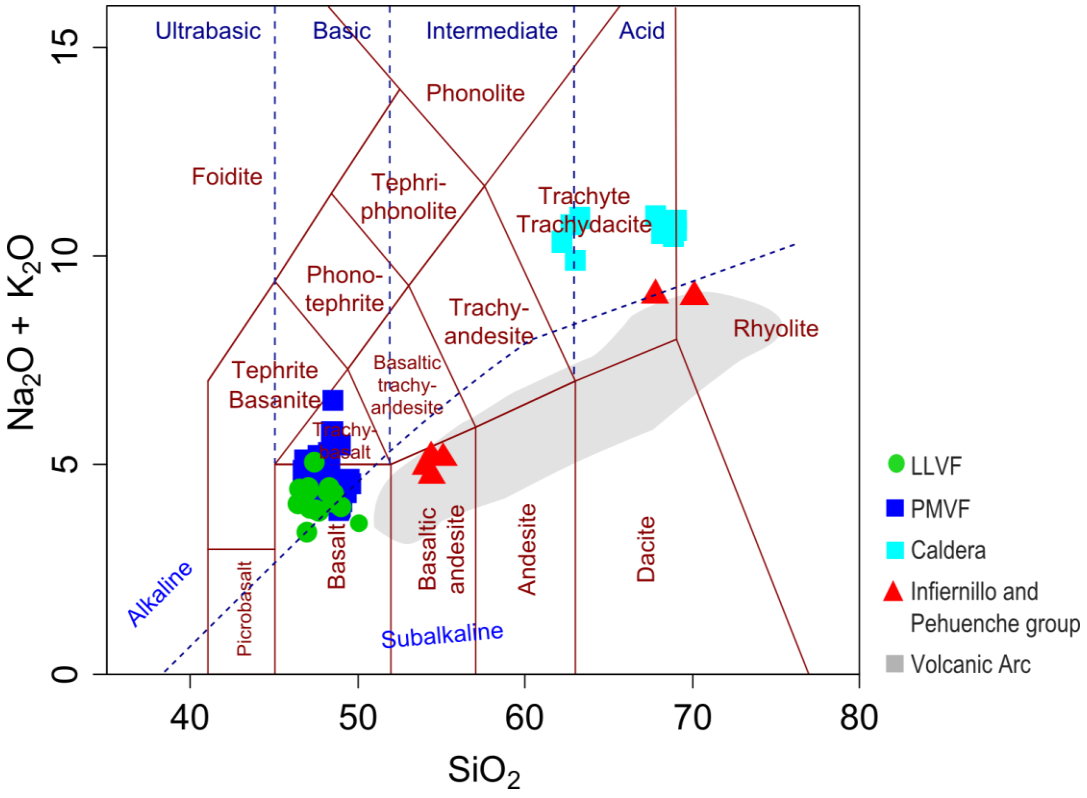

Figure 2.2. Total alkalies versus silica diagram (Le Bas et al., 1986). Most of the basalts and trachydacites from the back-arc are alkaline while the samples from the arc are sub-alkaline. The grey field corresponds to the Andean volcanic arc from the Mainz geochemical database (http://georoc.mpch-mainz.gwdg.de/georoc/Entry.html); only data from the region near our study area were included (34-39°S, 69-72°W).

The MgO content ranges from 4.5 to 12.2 wt % in basalts, from 4.6 to 5.7 wt % in intermediate samples and is <1% in the silicic samples (Figure 2.3). The average MgO content for basalts from Llancanelo volcanic field is 8.5 wt % while for the Payún Matrú volcanic field it is 6.8 wt %. The low MgO content in Los Volcanes group (LV1= 4.5 wt % and PN1= 5.4 wt %) from the Payún Matrú volcanic field are in agreement with the MgO content presented by Jacques et al. (2013) and Søager et al. (2013). The MgO content decreases in the Payún Matrú volcanic field from the Pampas Onduladas group with the highest MgO content (average 7.5 wt %); to the Río Grande, Payunia and Los Volcanes groups (average 6.1 wt %). In the case of the Llancanelo volcanic field, the MgO content decreases from the Carapacho group with the highest average MgO (9.9 wt %), to Malacara and Llancanelo groups (average 7.9 wt %) (Suplementary Table 2.1).

2.4.2.2 Trace elements

Rare earth element (REE) concentrations normalised to chondrites (Boynton, 1984) show a consistent pattern for the basalts from Llancanelo volcanic field and Payún Matrú volcanic field (Supplementary Table 2.1; Figure 2.4). All samples show enrichment in light rare earth elements (LREE) relative to heavy rare earth elements (HREE) as indicated by the La/Yb ratios (average Llancanelo volcanic field La/Yb = 9.14, Payún Matrú volcanic field La/Yb = 8.48). However, the Payún Matrú volcanic field has a steeper HREE pattern than the Llancanelo volcanic field as indicated by higher Dy/Yb (average Payún Matrú volcanic field Dy/Yb=2.25, Llancanelo volcanic field Dy/Yb = 2.18). Negative Eu anomalies, diagnostic of plagioclase crystallisation, are evident for the caldera group (Figure 2.4), as previously observed by Germa et al. (2010).

The majority of the basalts from the Llancanelo and Payún Matrú volcanic fields show enrichment in most of the incompatible elements compared to basalts from the Andean arc (Figure 2.5). The samples from the Llancanelo volcanic field compared to the Payún Matrú volcanic field present higher enrichment in the fluid-mobile elements Cs, Rb, Ba, U and Pb (Large Ion Lithophile Elements, LILE) and depletion in fluid-immobile elements Nb, Ta (High Field Strength Elements, HFSE) relative to LREE such as La, which are typical signatures of the volcanic arc (Jacques et al., 2013). Accordingly, Ba/Ta, La/Ta, Ba/Nb, La/Nb, and Th/Nb are higher in the arc and Infiernillo and Cerro Campanario-Pehuence groups than in the back-arc, and are slightly higher in the Llancanelo than in the Payún Matrú volcanic field (Figure 6a, b, f, g). On the Ba/Ta and La/Nb geospatial distribution maps, the lowest ratios are in the Payún Matrú and the Río Colorado volcanic fields, while these ratios increase towards the Llancanelo volcanic field and the arc (Figure 2.7a, b and 2.8a).

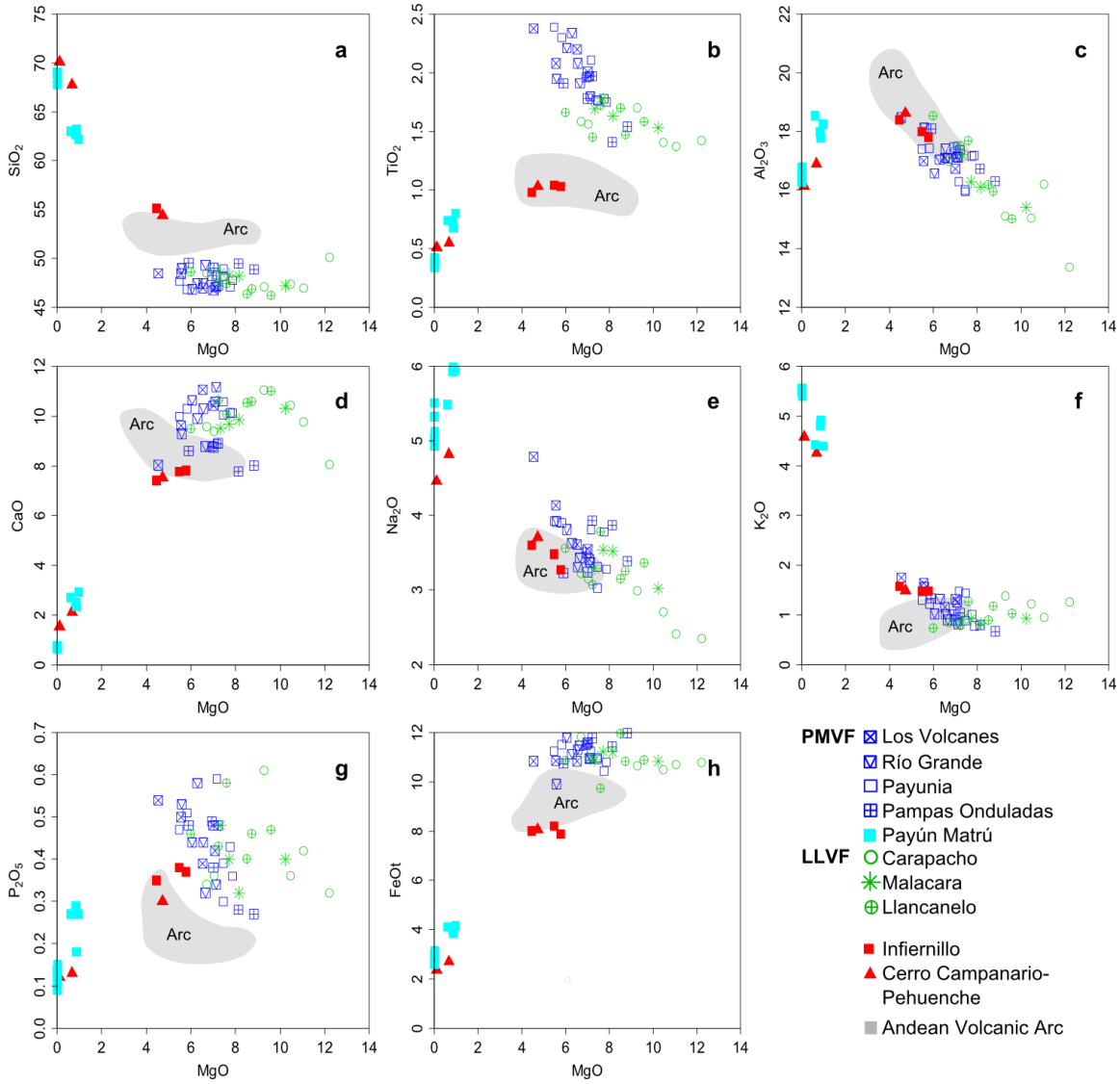

Figure 2.3. Major oxides versus MgO concentration (all in wt %). The Andean volcanic arc field corresponds to data from samples with SiO_2 ranging from 50.9 to 53.0 wt % from the Andean arc between 35°S and 38°S (Costa and Singer, 2002; Ferguson et al., 1992; Jacques et al., 2013; Lopez-Escobar et al., 1977; Tormey et al., 1991; 1995).

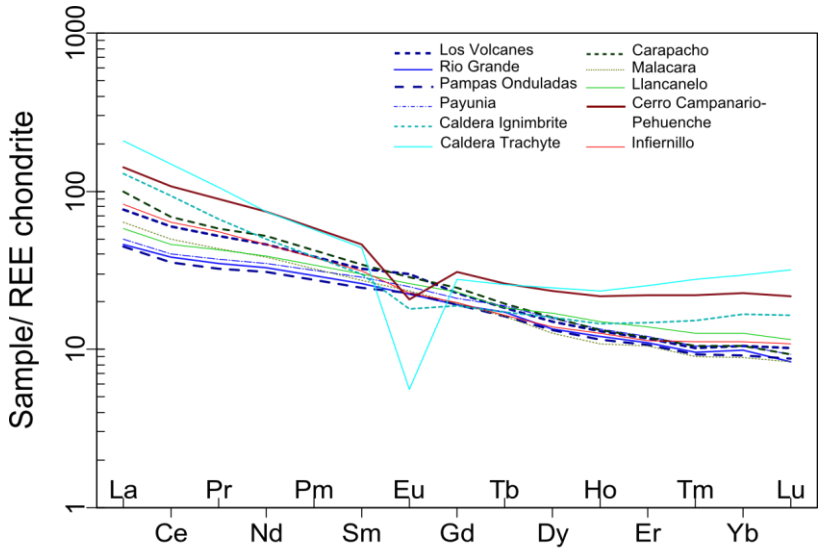

Figure 2.4. Rare earth element concentrations normalised to the chondrite values of Boynton (1984).

The basalts from the Payún Matrú volcanic field have higher Ta/Hf, Nb/Zr ,Ce/Pb, Nb/ Yb and Nb/Y, than the Llancanelo volcanic field; these ratios are highest in the Río Colorado volcanic field which is used in the present study as the local intraplate end-member with ocean island basalt (OIB)-like composition (Figure 2.6f) and may be associated with mantle upwelling (Søager et al., 2013). Basalts from the Llancanelo volcanic field show an intermediate composition between the arc and the OIB-like end-member (Figure 2.5 and 2.6a, c, d, e, f, g). Ce/Pb and Nb/Zr decrease in a westerly direction from the back-arc to the arc and from the Río Colorado northwards (Figure 2.7c, d). The Zr, Nb, and Ta contents increase southward, from Llancanelo to Payún Matrú volcanic fields (Figure 2.8 b, c, d). The Caldera group displays the lowest Ba/Ta and La/Ta ratios (Figure 2.6a) while this group shows the highest Ta/Hf and Nb/Yb (Figure 2.6 e, f) as a result of fractionation.

2.4.2.3. Sr isotopic ratios

The $^{87}Sr/^{86}Sr$ ratios show a restricted range of values, between 0.703747 and 0.704089 (Table 2.2). These values are similar to previous Sr-isotopic measurements reported in the same area (Hernando et al., 2012; Jacques et al., 2013; Muñoz et al., 1989; Pasquarè et al., 2008; Søager and Holm, 2013; Stern et al., 1990). These low Sr isotopic values are indicative of a mantle origin with little to no sialic crustal contamination.

Table 2.2. Sr isotope results for selected samples from the LLVF and the PMVF

Area	Group	Samples	$^{87}Sr/^{86}Sr$
PMVF	Los Volcanes	LV1	0.703858
PMVF	Río Grande	VRE12	0.704083
PMVF	Payunia	SM16	0.704027
PMVF	Payunia	SM18	0.704063
PMVF	Pampas Onduladas	VRE20	0.703747
LLVF	Carapacho	CP3	0.703846
LLVF	Malacara	MC5	0.704050
LLVF	Malacara	VRE27	0.703981
Retroarc	Infiernillo	VRE4	0.704089

2.5. Discussion

2.5.1. Arc influence in the Payenia Basaltic Province

The volcanic arc is characterised by enrichment in LILE relative to HFSE and LREE and enrichment in LREE relative to HFSE, therefore ratios such as Ba/Ta, La/Ta, Ba/Nb, La/Nb, and Th/Nb are high in the arc compared to the back-arc. The geospatial distribution maps illustrate an easterly decrease from the arc to the back-arc in these ratios (Figure 2.7a, b). This trend of decreasing arc signatures in an easterly direction away from the volcanic front is related to a decrease in the amount of slab-derived fluids or melts in the magmas (Jacques et al., 2013; Rivalenti et al., 2004; Stern et al., 1990). Furthermore, a N-S trend is also illustrated, as the Llancanelo volcanic field has higher enrichment in Ba and La relative to Ta and Nb than the

Payún Matrú volcanic field (Figure 2.7a and 2.8a). The Llancanelo volcanic field has a more pronounced arc signature than the Payún Matrú volcanic field as suggested by higher ratios of fluid-mobile to fluid-immobile elements and depletion in Nb and Ta. The Llancanelo volcanic field is interpreted to have a weak arc signature as shown by moderate Ba/Ta (>500), high La/Ta (>24), La/Nb (>1.5), Th/Nb (>0.25) and low Nb/U (<20), Ta/Hf (<0.21), Nb/Yb ratios (< 6.5), in addition to negative Nb, Ta and Ti anomalies.

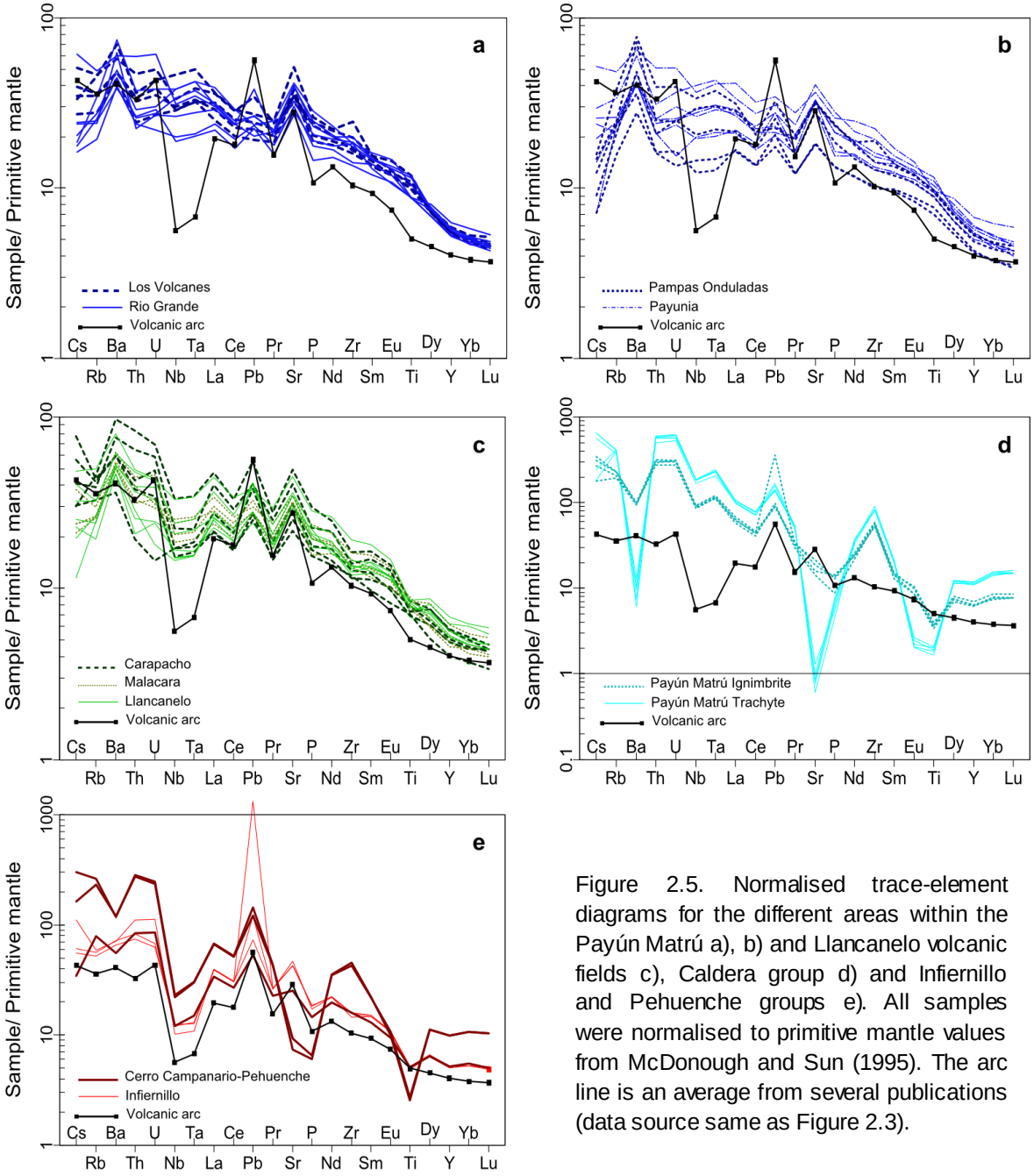

Figure 2.5. Normalised trace-element diagrams for the different areas within the Payún Matrú a), b) and Llancanelo volcanic fields c), Caldera group d) and Infiernillo and Pehuenche groups e). All samples were normalised to primitive mantle values from McDonough and Sun (1995). The arc line is an average from several publications (data source same as Figure 2.3).

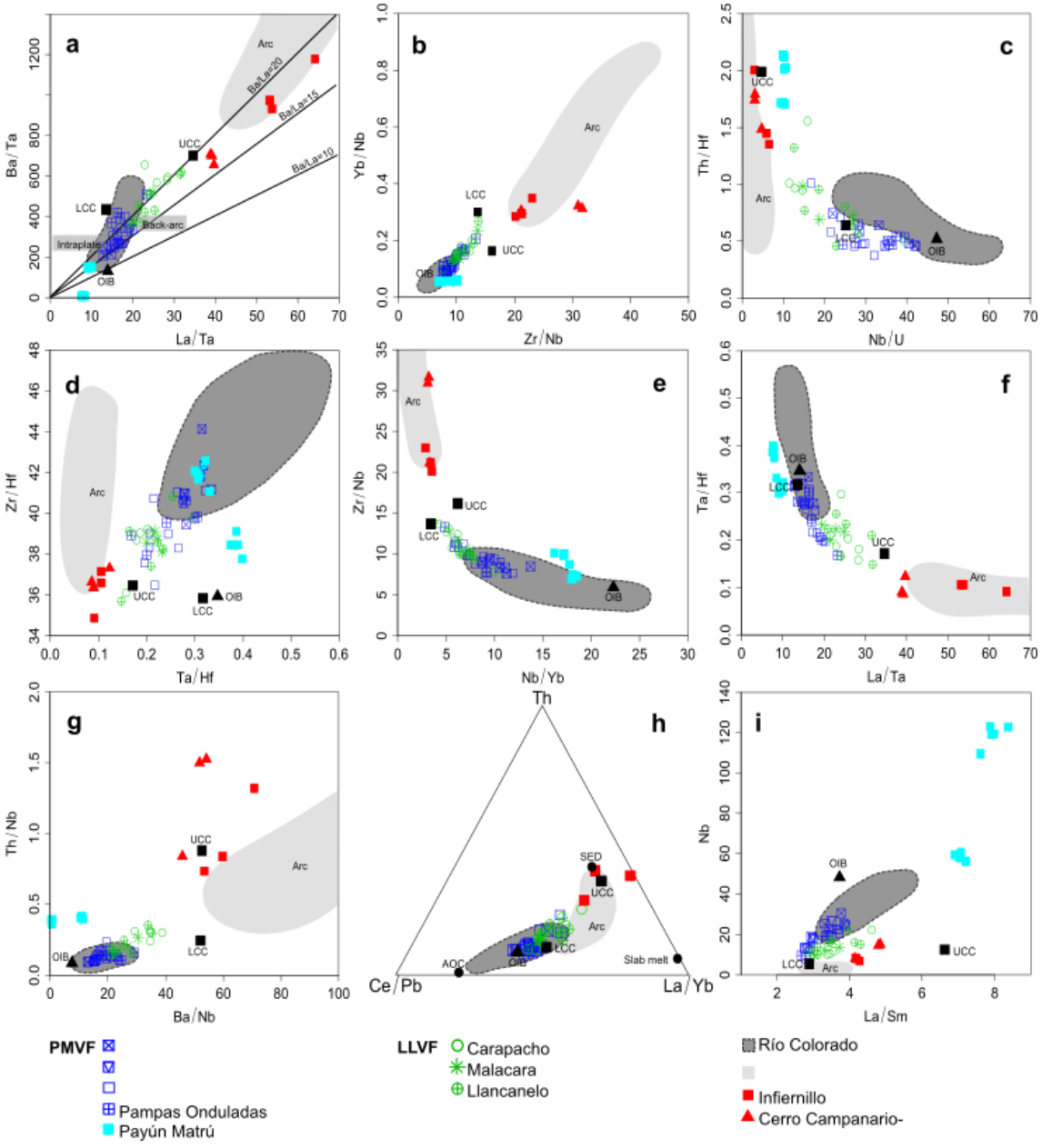

Figure 2.6. Trace-element ratio diagrams, a) La/Ta vs Ba/Ta, b) Zr/Nb vs Yb/Nb, c) Nb/U vs Th/Hf, d) Ta/Hf vs Zr/Hf, e) Nb/Yb vs Zr/Nb, f) La/Ta vs Ta/Hf, g) Ba/Nb vs Th/Nb, h) ternary diagram of Ce/Pb, Th concentration and La/Yb, i) La/Sm vs Nb. The symbols are as in Figure 2.3. The arc field is compiled from several publications (data source same as Figure 2.3). The dark grey field corresponds to the Río Colorado volcanic field (data from Søager et al., 2013) and represents the local intraplate end-member. Compositions for the upper continental crust (UCC) and the lower continental crust (LCC) are from Rudnick and Gao (2003). Composition for the OIB is from Sun and McDonough (1989). Values for slab melt, sediment from the subducting Nazca plate (SED) and altered oceanic crust (AOC) are from Jacques et al. (2013). Note that differentiated samples from the Payún Matrú caldera have been included therefore Ba/Ta, La/Ta, Th/Hf and Ba/Nb ratios are especially modified by fractional crystallisation.

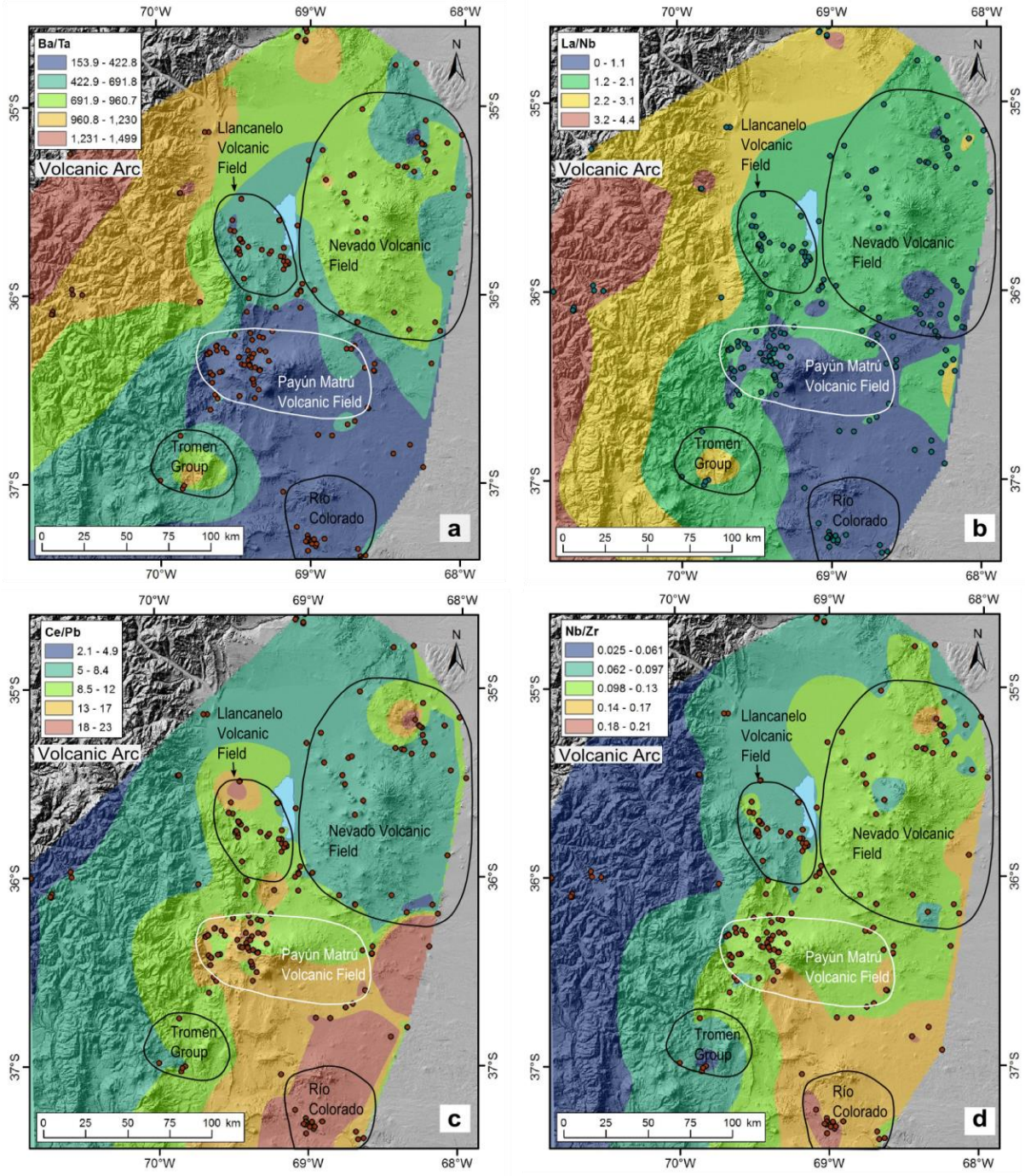

Figure 2.7. Geospatial distribution of trace-element ratios. a) Ba/Ta, b) La/Nb, c) Ce/Pb, and f) Nb/Zr. The trace-element spatial distribution ratios were created using a natural neighbourhood, interpolation tool from ArcMap10. The data points used for these maps were obtained from this investigation as well as from Bertotto et al. (2009), Costa and Singer (2002), Ferguson et al. (1992), Germa et al. (2010), Jacques et al. (2013), Pasquarè et al. (2008), Søager et al. (2013) and Tormey et al. (1991; 1995) and were selected to have SiO_2 <53 wt %. For all the maps, approximately 255 data points were used except for Ce/Pb for which 230 data points were used. The background image used for all of the maps is a hill-shaded SRTM (Shuttle Radar Topography Mission).

In a Ba/Ta vs La/Ta diagram (Figure 2.6a), used among Patagonian back-arc basalts to discriminate between arc, back-arc and intraplate basalts (Kay et al., 2006a), the groups from the Llancanelo volcanic field show a broad distribution and are closer to the arc end-member than the Payún Matrú volcanic field groups. On the same diagram, the Payún Matrú volcanic field groups overlap with the composition of the local intraplate basalts, suggesting no association with the arc (Figure 2.6a). In a Ba/Nb vs Th/Nb diagram (Figure 2.6g), the samples from the Llancanelo volcanic field display a positive trend towards the arc composition, showing higher Ba and Th relative to Nb. Furthermore, the high Th content is demonstrated by the displacement of all the Llancanelo volcanic field groups to a higher Th content (Figure 2.6h and 2.9d). In addition, the Llancanelo volcanic field groups are above the mid ocean ridge-ocean island basalt array (MORB-OIB array; Figure 2.9b) as Th is incorporated from slab components. The Carapacho and Llancanelo groups have the highest Th content of all basaltic groups (averages 3.6 and 3.8 ppm respectively). The high Th concentration among these groups does not result from enrichment during crystallisation because these samples have high MgO contents. The high Th concentration is not likely to be linked to slab dehydration as Th is highly immobile in hydrous fluids (Turner et al., 2003). The location of the subducting slab in the back-arc at this latitude is not well defined, however it has been inferred to be approximately 200 km deep (Tassara et al., 2006), it is improbable that dehydration of the slab will still be occurring (Turner et al., 2003) at such depth. Moreover, a fluid-sensitive ratio such as Sr/Th (Dosseto et al., 2003) is relatively lower for the Llancanelo volcanic field (average Sr/Th= 195, 244, 251 for Carapacho, Llancanelo and Malacara groups, respectively) compared to the Andean arc (average Sr/Th = 283) suggesting that the weak arc signature observed is not likely to be related to fluids released from the slab.

The basalts from the Llancanelo volcanic field trend towards a higher La/Yb at higher Th and lower Ce/Pb than the basalts from the Payún Matrú volcanic field, locating the Llancanelo volcanic field close to the arc-like composition and between the slab melts and the slab sediments end-members (Figure 2.6h). Slab partial melts can fractionate and transport Th and LREE (Kessel et al., 2005) and are characterised by their high residual garnet signature which is reflected in high La/Yb, Sm/Yb and Dy/Yb as HREE are compatible in garnet (La/Yb=100, Sm/Yb=25, Dy/Yb= 6.8, based on slab melt values from Jacques et al., 2013). A strong depletion in HREE associated with slab-derived partial melts is not characteristic of the basalts from the Llancanelo volcanic field. Slab partial melts have previously been suggested for some volcanic segments of South America such as the Austral Volcanic Zone (Figure 2.1; Sigmarsson et al., 1998) and the Southern Volcanic Zone (Figure 2.1; Jacques et al., 2013), where lavas are characterised by high Th concentrations, La/Yb and Sr/Y ratios and low Ce/Pb ratios. It is unclear if slab partial melting is a valid hypothesis for the Llancanelo volcanic field as lavas in this region have low La/Yb and Sr/Y ratios, while the Th content is relatively high (average Th in Llancanelo volcanic field = 3.22 ppm). The Ce/Pb ratio is not a good discriminatory parameter for slab melting in our study area, because of evidence for lower crustal contamination which affects this ratio (Søager et al., 2013) (see Section 2.5.2). The slab

melt influence can also be determined by using U-series radioactive disequilibrium, which can be employed as a tracer for magma generation processes such as in the Austral Volcanic Zone (Sigmarsson et al., 1998). In this study, U-series analyses were not carried out. However, it will be desirable in future investigations, in order to fully assess the hypothesis of partial melting of the subducting slab.

The sediment component has high Ba/Ta, Ba/La, Th/Ta and Th/La than the altered oceanic crust (AOC values from Jacques et al., 2013) and has lower Nb/Yb, Sr/Th and Dy/Yb than any other slab component. The groups from the Llancanelo volcanic field follow this trend possibly indicating that the arc signature could be related to source input of sediment melts from the slab (Figures 2.6, 2.7, 2.9) while Payún Matrú volcanic field dies not. In addition, the groups from Llancanelo volcanic field are displaced to a higher Th/Nb at a higher Th content than the Payún Matrú volcanic field, also suggesting that the slab component observed in the Llancanelo volcanic field can be associated to sediment melting in order to transport Th (Figure 2.9d).

2.5.2. Geochemical variations in the continental back-arc and possible causes

The Llancanelo and Payún Matrú volcanic fields have some geochemical similarities such as having alkaline basalts and trachybasalts with a restricted SiO_2 content (46.2 – 50.0 wt %; Figure 2.2). However, the two volcanic fields have distinct geochemical features suggesting different magmatic sources. In the previous section, it was established that the Llancanelo volcanic field has a weak arc signature possibly attributed to sediment melts transported from the slab, while the Payún Matrú volcanic field does not show such signatures.

The Llancanelo volcanic field shows little to no overlap with the local intraplate composition (Río Colorado volcanic field; Søager et al., 2013), situating this volcanic field at an intermediate composition between the arc and the local intraplate end-members. Geochemical signatures such as low Sm/Yb, Sr/Y and Ce/Pb observed especially in the Carapacho and Llancanelo groups from the Llancanelo volcanic field compared to the local OIB-like can be the result not only of slab sediment melts but also of lower continental crust assimilation. The lower continental crust (LCC, Rudnick and Gao, 2003) is depleted in K, Rb, Ba, Zr, Hf, Th, U and LREE relative to the average arc, the OIB and slab components such as sediments and slab melts. The Llancanelo volcanic field samples have Zr and Hf depletion (Figure 2.5, only Zr shown) while the remaining elements (Rb, Ba, Pb, Th, U) are enriched in relation to the Payún Matrú volcanic field. They are best explained by the contribution of slab-derived sediments as previously discussed. Intermediate Th/Nb and La/Nb ratios can be diagnostic of lower crustal assimilation, as these ratios initially low in the mantle-derived magmas, increase during crustal assimilation. In a diagram of Nb/U vs Ce/Pb (Figure 2.9a) the arc and the local intraplate end-members are well differentiated and form a linear trend. Samples from the Llancanelo volcanic field also show a linear trend but they are shifted towards the LCC end-member. This shift to a higher Nb/U values is interpreted as an indication of lower crustal assimilation, taking place possibly in both volcanic fields. The Ba/Th vs Sr/Th diagram also shows a similar shift towards

higher Ba/Th, supporting a crustal assimilation hypothesis, in particular for the Pampas Onduladas group (Figure 2.9c). The Llancanelo volcanic field groups are shifted towards the LCC and with an intermediate composition between the MORB-OIB array and the average Andean arc composition (Figure 2.9b). Lower continental crust contamination was previously suggested by Søager et al. (2013) for this volcanic field where they suggested up to 70% of lower continental crust assimilation in the Nevado volcanic field (Figure 2.1).

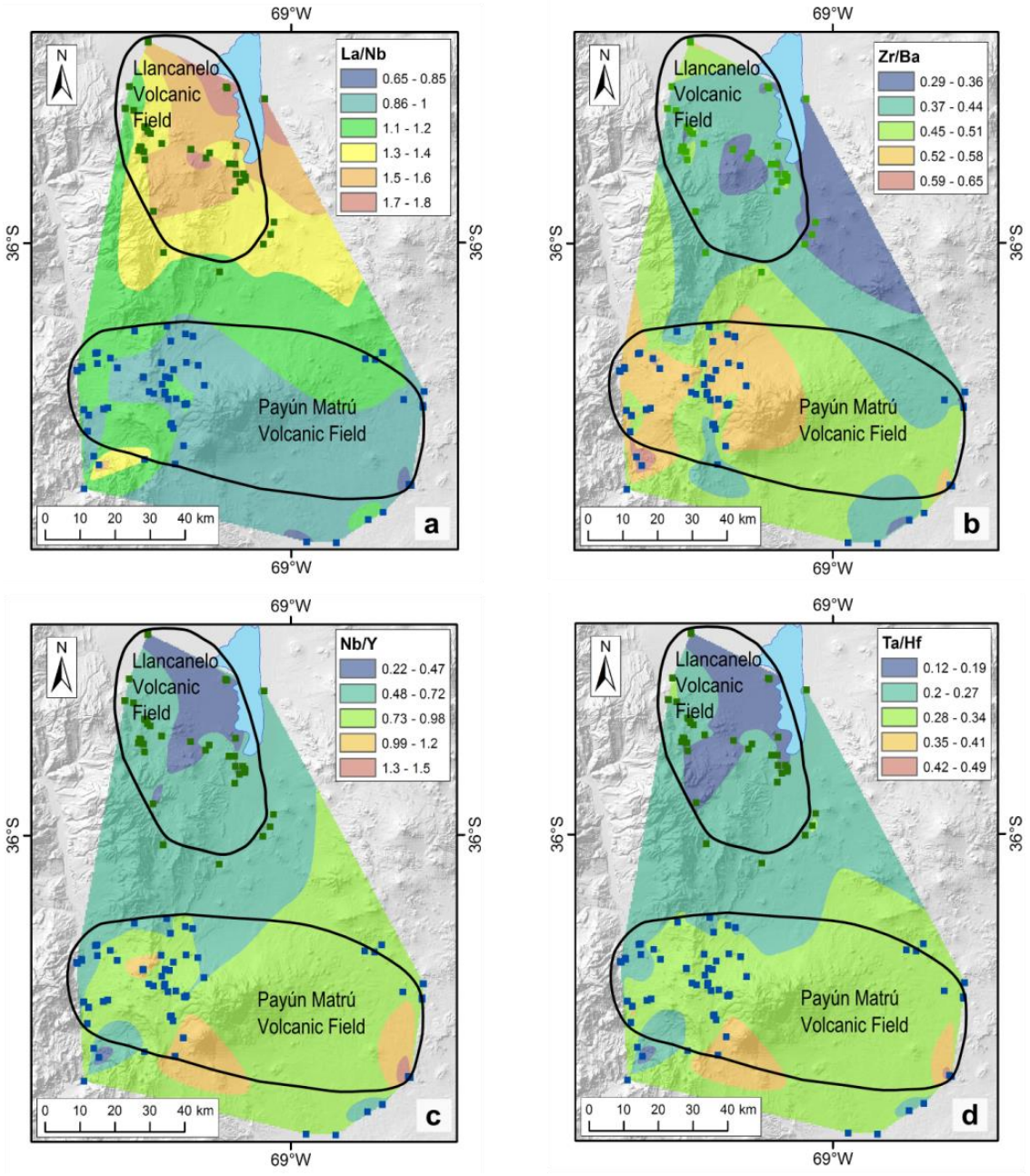

Figure 2.8. Localised geospatial distribution maps of trace-element ratios. a) La/Nb, b) Zr/Ba, c) Nb/Y, and d) Ta/Hf. The data points used are from this study as well as Germa et al. (2010), Jacques et al. (2013) and Søager et al. (2013). These maps are based on 112 data points.

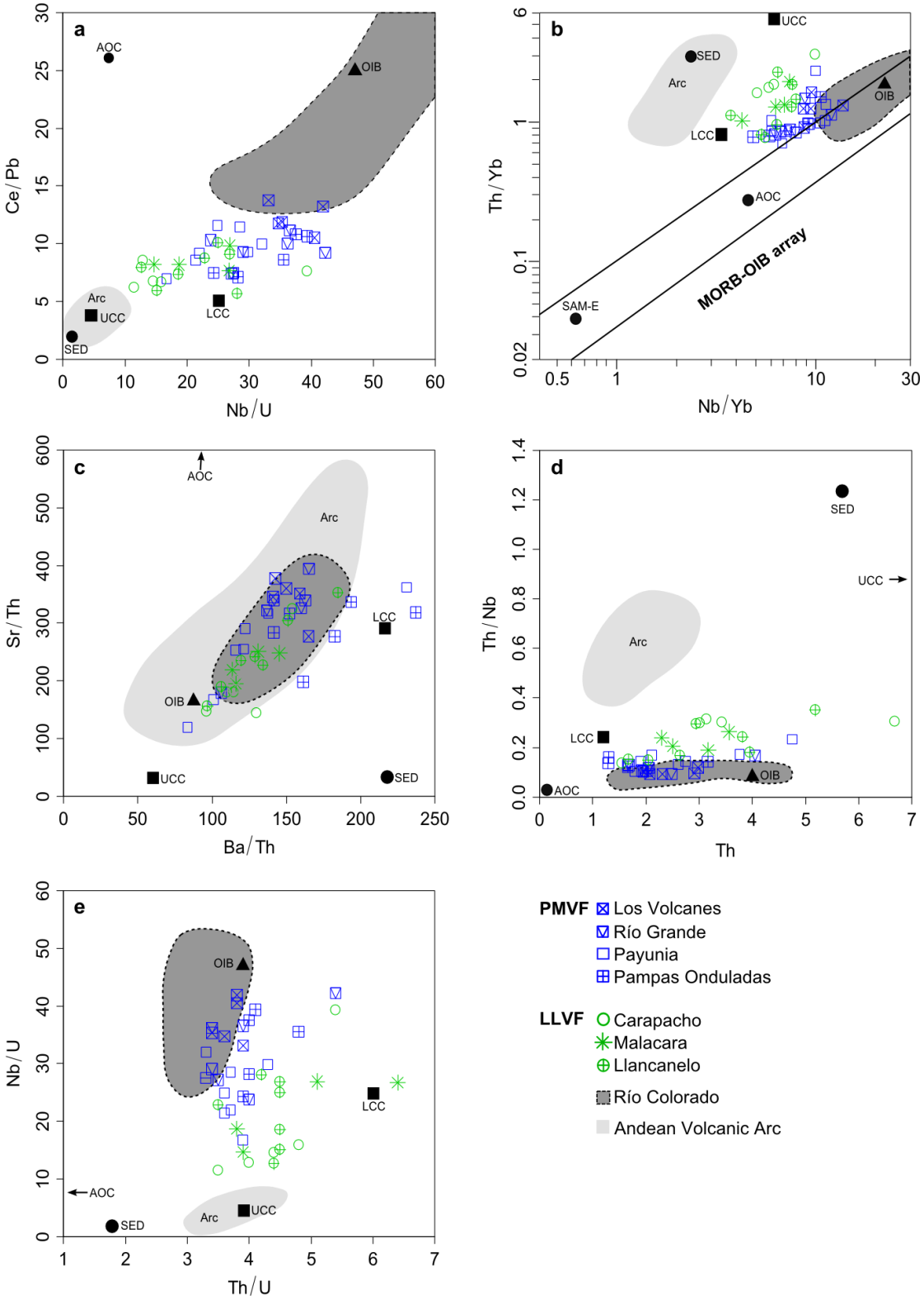

Figure 2.9. Trace-element diagrams. a) Nb/U vs Ce/Pb (modified from Jacques et al., 2013) wherein a shift to the right towards a higher Nb/U is interpreted as lower continental crust assimilation. b) Nb/Yb vs Th/Yb (modified from Pearce, 2008), c) Ba/Th vs Sr/Th, d) Th vs Th/Nb and e)Th/U vs Nb/U. Reference as in Figure 2.3 (Arc field) and Figure 2.6.

In addition, it is important to consider that geochemical signatures from the LCC and melts related to the lithospheric mantle can be similar. The contribution from the sub-continental lithospheric mantle has been inferred in the back–arc of southern Mendoza based on O, Nd and Hf isotopes (Jacques et al., 2013). However, Søager et al. (2013) attributed the feldspar signature, indicated by positive Ba, K, Sr and Eu anomalies in the affected basalts, to the lower continental crust, as feldspars are not stable in the lithospheric mantle. Melting of the lithospheric mantle would result in a weaker garnet signature than deeper asthenospheric melts and high Th/U ratios up to 7.5 (Bourdon and Sims, 2003). The Th/U ratios in the Llancanelo and the Carapacho groups are in many cases high and range up to 6.4. However, high Th/U ratios could also be generated by lower crustal assimilation since the lower crust commonly has a Th/U value of 6. Overall, the data suggest that the geochemical signatures observed in the Llancanelo volcanic field magmatic source were modified by several processes such as a slab component (sediment melts from the slab) and lower crustal contamination. Lithospheric mantle melts may have also contributed to the Llancanelo volcanic field magmas, however further investigation is required to test this hypothesis.

The basalts from the Payún Matrú volcanic field are enriched in most of the immobile elements, such as Nb, relative to the Llancanelo volcanic field and the Andean arc basalts (Figures 2.6i). Nevertheless, the strongest Nb enrichment is shown among the Río Colorado basalts. This was previously interpreted by Jacques et al. (2013), Kay et al. (2006a) and Søager et al. (2013) as due to derivation from an enriched mantle. Thus, here we used the composition of the Río Colorado volcanic field, as the local intraplate end-member. The basalts from the Payún Matrú volcanic field have a similar composition to that of the Río Colorado field (Figure 2.6) suggesting that the general magmatic source for this volcanic field could also be the same enriched mantle (Jacques et al., 2013; Søager and Holm, 2013). The samples from Los Volcanes group show the greatest Zr, Nb, Hf and Ta enrichment among groups of the Payún Matrú volcanic field as indicated by high Ta/Hf (0.29) resembling the values observed in the local intraplate end-member (Río Colorado basalts, Ta/Hf = 0.41). Most of the samples from Los Volcanes group are placed within the Río Colorado field (Figure 2.6), and are within the MORB-OIB array (Figure 2.9b; Pearce, 2008).

Our Sr isotope data show a restricted range and are in agreement with previous data reported for basalts in the Payenia basaltic province (Bertotto et al., 2009; Hernando et al., 2012; Jacques et al., 2013; Kay et al., 2004; Paquarè et al., 2008; Søager and Holm, 2013; Stern et al., 1990). The low Sr isotope ratios suggest little scope for sialic crustal contamination. Accordingly, Hernando et al. (2012) concluded that any crustal contamination in the Payún Matrú caldera would have been small as it is not reflecting an increase in radiogenic ^{87}Sr among the basalts. Furthermore, Eby (1990) determined that A-type (intraplate setting) granitoids derived from an OIB source result in constant Y/Nb and Yb/Ta <1.2 and low Sr isotopic ratios. The silicic Caldera group presents Y/Nb and Yb/Ta ratios <1.2, further supporting the association of these volcanic rocks with an initial intraplate mantle source. In order to determine

the possibility of upper crustal contamination in this volcanic field it is recommended to use another isotopic system with a shorter time-scale such as Th and U or stable isotopes such as $\delta^{18}O$.

2.5.3. Slab geometry and Payenia Basaltic Province volcanism

The variable geochemical signatures observed in the continental back-arc can be related to geometrical changes in the subducting slab. This area of the continental back-arc experienced an episode of shallow subduction peaking in the late Miocene associated with compressional deformation of the overriding plate and an eastward migration of the volcanic arc (Kay and Copeland, 2006; Kay et al., 2006a, b). During the Pliocene and Quaternary, the angle of subduction increased producing the retreat of the volcanic arc to its current location and resulting in mild extension of the overriding plate (Kay et al., 2006a). This mild extension has been linked to slab roll-back as inferred from the migration of back-arc volcanism in the Nevado Volcanic field towards the N-W from ~2.8 Ma to 0.5 Ma (Gudnason et al., 2012). This is also shown by the geospatial distribution maps where the Nevado volcanic field has higher Ba/Ta and lower Ce/Pb than Llancanelo and Payún Matrú volcanic fields (Figure 2.7a, c). The slab roll-back results in extension and provides the necessary space for mantle up-welling. However, it is unclear why the Llancanelo volcanic field does not show high enrichment in HFSE such as in the Payún Matrú volcanic field when they are located only ~30 km apart. One of the possible explanations is that the strong intraplate signature has been overprinted by the components present in the Llancanelo volcanic field such as lower continental crust assimilation and slab components. Another possibility is that because the Llancanelo volcanic field is located closer to the present Pampean flat slab (~270 km north of the Llancanelo volcanic field; Figure 2.1) than the Payún Matrú volcanic field, this colder area could act as a barrier for an ascending enriched mantle. This is supported by the geospatial distribution maps showing a N-S trend in the continental back-arc with an increase in Nb and Zr content from north to south (Figure 2.8). This N-S trend observed in the geochemical distribution maps correlates with a decrease in lithospheric thickness as the lithosphere-athenosphere boundary (LAB) depth decreases from the north-east cold dense flat slab portion (~120 km) to the south-west (~60 km), therefore having a shallower asthenosphere (Tassara et al., 2006). By decreasing the lithospheric mantle thickness, heat flow convection is induced therefore increasing the temperature in the back-arc.

2.6. Conclusions

Continental back-arc magmas of the Payenia Basaltic Province are influenced by several constituents such as (i) slab component (such as: slab fluids and/or sediment melts), (ii) lower crustal contamination, and (iii) an enriched intraplate mantle source (Jacques et al., 2013; Søager et al., 2013). Nevertheless, the influences of these constituents vary across the several volcanic fields of this region. The Llancanelo volcanic field shows evidence of a weak arc signature. This arc signature in the Llancanelo volcanic field is not likely to be related to slab dehydration, as inferred from the slab location and the enrichment in less fluid-mobile Th

relative to U (Figure 2.9e). Instead, the influence from subduction components in the Llancanelo volcanic field lavas can be dominated by the contribution of subducted sediments. The absence of HREE depletion argues against the involvement of slab partial melts which is another possible slab component. On the geospatial distribution maps, the Ba/Ta and La/Nb ratios decrease from the Andean arc in an easterly direction. These ratios also decrease from north to south, reflecting the absence of a slab influence in the Payún Matrú volcanic field lavas, while high Nb/U values at a given Ce/Pb could suggest the occurrence of lower crustal assimilation. However, the Sr isotope data do not suggest sialic crustal contamination. In particular, Los Volcanes group shows high Zr/Ba, Nb/Y, Ce/Pb, Nb/Yb and Ta/Hf ratios similar to the local intraplate end-member. Geochemical maps show that while an enriched mantle signature is observed for the Payún Matrú volcanic field, it is diminished in the Llancanelo volcanic field. Thus, geochemical mapping could be used to help identify areas of elevated concentration of high field strength element coinciding with areas of mantle upwelling.

Supplementary Table 2.1. Major- and trace-element results from samples analysed. Major-elements in wt % and trace-elements in ppm

Sample	LV6	LV1	LV3	LV8	PN1	RG1	RG2	RG5	RG11	LV9	VRE12
SiO_2	46.83	48.34	46.95	46.06	47.33	49.02	47.76	48.39	46.95	46.92	46.77
TiO_2	2.20	2.38	1.97	1.98	2.02	2.15	2.40	1.75	2.28	1.72	1.76
Al_2O_3	17.06	18.42	17.09	16.49	16.57	16.55	17.44	15.83	17.49	15.49	17.03
FeO_t	10.81	10.81	10.92	11.45	10.45	11.43	11.27	10.82	11.30	10.78	10.37
MnO	0.15	0.15	0.15	0.16	0.15	0.16	0.15	0.15	0.15	0.16	0.16
MgO	6.52	4.53	7.06	6.91	5.36	7.27	5.48	7.39	5.85	7.33	7.70
CaO	11.04	8.01	10.55	10.28	9.35	9.02	10.02	10.49	10.24	9.77	10.08
Na_2O	3.60	4.78	3.40	3.50	4.01	3.87	3.94	3.00	4.00	3.21	3.75
K_2O	1.15	1.74	1.24	1.30	1.60	1.49	1.30	0.87	1.21	1.40	1.00
P_2O_5	0.38	0.54	0.42	0.48	0.49	0.60	0.48	0.30	0.51	0.38	0.42
Total	99.52	99.49	99.42	98.23	97.09	101.5	100.2	99.08	99.94	98.56	99.93
V	298	238	259	262	252	222	272	239	262	232	251
Cu	49	29	46	48	42	40	37	60	56	55	74
Zn	55	56	55	54	54	62	58	59	56	53	69
Ga	19.9	20.8	18.9	19.2	20.1	19.8	21.0	19.7	20.4	18.9	19.6
Rb	16.7	27.1	20.8	21.4	27.9	20.6	16.5	14.9	15.3	29.4	14.5
Sr	701	1023	753	694	631	826	797	537	782	565	647
Y	23.6	23.8	23.1	23.7	25.4	25.0	24.9	22.4	24.2	22.8	26.8
Zr	168	258	181	174	208	192	209	142	184	191	196
Nb	18.8	30.4	19.8	19.1	22.0	25.2	25.2	12.4	22.3	20.4	17.3
Cs	0.57	0.70	0.73	0.83	1.07	0.39	0.43	0.51	0.37	1.29	0.50
Ba	292	462	317	317	379	491	325	256	295	396	413
Sc	36.5	21.1	33.4	31.3	27.5	25.7	30.3	33.0	28.6	30.4	33.3
La	16.3	23.6	18.8	20.5	23.2	25.2	20.0	14.2	20.4	19.5	18.8
Ce	33.7	48.2	38.0	42.4	47.3	48.4	40.0	28.8	41.4	39.7	39.6
Pr	4.73	6.34	5.13	5.64	6.13	6.27	5.48	4.00	5.55	5.06	5.41
Nd	22.4	27.7	23.4	25.2	27.2	28.8	25.0	18.9	25.4	22.0	24.2
Sm	5.55	6.28	5.46	5.86	6.30	6.56	6.04	4.86	5.94	5.27	6.01
Eu	1.87	2.21	1.83	1.82	1.93	2.27	2.06	1.66	2.00	1.62	1.98
Gd	5.59	5.85	5.33	5.81	5.91	6.39	5.97	5.25	5.91	5.07	6.29
Tb	0.92	0.87	0.88	0.90	0.94	0.96	0.92	0.80	0.89	0.81	0.92
Dy	4.83	4.85	4.84	4.87	5.09	5.16	5.06	4.56	5.07	4.59	5.38
Ho	0.95	0.93	0.91	0.93	0.99	0.99	0.97	0.92	0.96	0.90	1.06
Er	2.54	2.46	2.44	2.50	2.73	2.58	2.57	2.38	2.52	2.47	2.95
Tm	0.33	0.33	0.32	0.33	0.37	0.33	0.33	0.30	0.33	0.34	0.41
Yb	2.15	2.21	2.09	2.20	2.32	2.24	2.26	2.07	2.12	2.05	2.55
Lu	0.29	0.33	0.32	0.31	0.35	0.31	0.33	0.29	0.32	0.31	0.36
Hf	4.25	5.84	4.42	4.29	5.08	4.67	4.99	3.63	4.34	4.70	4.80
Ta	1.20	1.84	1.22	1.19	1.42	1.56	1.56	0.75	1.39	1.29	1.03
Pb	2.87	4.06	3.31	3.66	5.16	3.52	3.03	3.37	3.94	5.71	3.98
Th	1.95	2.91	2.60	2.74	3.76	2.98	2.31	2.11	2.07	4.75	1.79
U	0.54	0.86	0.70	0.77	1.00	0.76	0.60	0.58	0.55	1.22	0.54

Major-element oxide analysis: School of Earth and Environmental Sciences, University of Wollongong, Australia

Trace-element analysis: Research School of Earth Sciences, Australian National University, Canberra , Australia

Note: The average MgO in wt % for each group classification is, Los Volcanes = 6.08, Río Grande = 7.02, Payunia = 7.47, Pampas Onduladas = 7.47, Caldera = 0.66, Carapacho = 9.86, Malacara = 8.39, Llancanelo = 7.87, Infiernillo = 5.26, Cerro Campanario-Infienillo = 1.90.

Supplementary Table 2.1. (cont)

Sample	VRE13	VRE37	VRE38	VRE40	SM16	SM17	SM18	VRE19	VRE20	VRE21	VRE46a
SiO_2	49.15	48.45	49.82	49.20	46.26	46.27	46.94	48.31	49.71	49.34	50.05
TiO_2	1.80	2.13	1.98	1.91	2.28	2.19	1.79	2.01	2.02	1.90	1.82
Al_2O_3	17.70	17.78	18.45	17.04	16.62	16.37	17.07	17.78	17.99	18.03	17.59
FeO_t	11.13	11.56	10.09	11.45	10.86	11.65	10.94	12.07	11.84	10.71	11.79
MnO	0.15	0.15	0.15	0.15	0.15	0.16	0.15	0.16	0.15	0.14	0.15
MgO	8.11	6.70	5.69	6.64	6.14	5.98	7.12	7.39	7.15	5.88	7.16
CaO	10.42	10.53	9.45	8.76	9.66	10.52	11.16	9.13	9.06	8.59	8.93
Na_2O	3.38	3.38	3.99	3.43	3.54	3.77	3.37	4.03	3.61	3.22	3.31
K_2O	0.80	1.04	1.59	0.90	1.29	1.01	0.82	1.06	1.04	1.33	0.91
P_2O_5	0.37	0.45	0.54	0.32	0.56	0.43	0.34	0.49	0.51	0.48	0.39
Total	102.8	101.7	101.5	99.37	98.97	99.03	100.2	102.0	103.1	102.0	102.3
V	255	264	257	214	251	278	270	221	225	242	221
Cu	61	59	47	47	46	50	51	47	46	57	53
Zn	61	62	59	67	57	60	56	64	66	65	69
Ga	20.4	20.9	21.1	20.2	20.8	20.1	20.1	20.5	20.0	20.8	20.0
Rb	11.7	14.7	29.0	14.2	20.2	15.7	12.8	14.5	14.8	22.8	12.7
Sr	600	653	727	570	808	660	653	642	638	626	557
Y	24.2	25.7	28.8	22.7	24.5	25.2	21.6	23.5	23.1	22.6	20.8
Zr	148	160	234	134	202	170	139	148	149	199	135
Nb	13.2	18.2	24.2	13.1	26.6	17.4	12.8	19.0	19.3	22.3	13.6
Cs	0.34	0.41	1.09	0.15	0.62	0.54	0.50	0.30	0.31	0.33	0.19
Ba	261	272	430	273	396	280	273	308	475	510	320
Sc	34.6	34.3	30.9	25.1	27.9	32.6	34.8	25.0	25.8	28.2	25.4
La	15.5	17.3	27.0	13.6	21.9	17.9	14.2	18.7	18.4	20.4	14.0
Ce	32.5	35.7	53.4	28.1	46.1	38.8	30.9	37.6	36.0	34.4	28.6
Pr	4.53	4.93	7.06	4.05	5.97	5.24	4.23	4.99	4.88	5.12	3.93
Nd	20.9	22.7	30.9	19.2	26.8	23.9	19.8	23.2	22.4	23.3	18.5
Sm	5.61	5.84	6.93	4.95	6.27	5.99	5.05	5.64	5.45	5.61	4.80
Eu	1.82	1.96	2.20	1.73	2.06	1.89	1.63	1.86	1.83	1.84	1.66
Gd	5.44	6.00	6.80	5.38	6.03	5.87	4.96	5.53	5.42	5.29	4.95
Tb	0.89	0.95	1.06	0.85	6.87	0.97	0.82	0.89	0.85	0.86	0.77
Dy	5.03	5.42	5.84	4.78	4.91	5.13	4.30	4.93	4.66	4.61	4.29
Ho	0.96	1.03	1.14	0.90	1.00	1.03	0.86	0.91	0.91	0.86	0.83
Er	2.54	2.77	3.06	2.39	2.50	2.63	2.30	2.53	2.43	2.35	2.23
Tm	0.34	0.37	0.41	0.31	0.34	0.35	0.31	0.33	0.31	0.33	0.30
Yb	2.20	2.30	2.74	1.97	2.22	2.34	2.05	2.08	2.09	2.11	1.92
Lu	0.30	0.33	0.40	0.29	0.32	0.31	0.27	0.29	0.29	0.31	0.28
Hf	3.95	4.18	5.71	3.66	4.92	4.36	3.63	3.73	3.75	4.90	3.40
Ta	0.77	1.11	1.51	0.79	1.59	1.07	0.75	1.14	1.13	1.38	0.82
Pb	3.50	3.20	5.19	3.05	4.61	4.18	4.17	3.47	3.39	4.84	3.83
Th	1.90	1.92	4.05	1.68	2.48	2.05	1.66	2.03	2.00	3.16	1.66
U	0.44	0.50	1.02	0.31	0.73	0.60	0.47	0.51	0.49	0.79	0.50

Supplementary Table 2.1. (cont)

Sample	VRE47	VRE49	VRE31	VRE33	VRE34	VRE35	VRE36	VRE39	LV5	LC1	LC2
SiO_2	50.70	49.34	68.46	69.62	69.83	70.07	67.87	63.21	61.48	62.34	62.01
TiO_2	1.60	1.41	0.42	0.39	0.37	0.34	0.40	0.74	0.79	0.67	0.72
Al_2O_3	16.91	16.68	16.94	16.69	16.44	16.65	16.71	18.60	18.04	17.51	17.79
FeO_t	12.43	11.40	3.07	2.86	2.80	2.62	3.12	4.12	4.10	3.78	3.96
MnO	0.15	0.15	0.12	0.11	0.11	0.11	0.14	0.10	0.10	0.10	0.10
MgO	9.15	8.11	0.008	0.008	0.008	0.008	0.02	0.61	0.96	0.86	0.84
CaO	8.31	7.75	0.76	0.74	0.70	0.64	0.68	2.71	2.89	2.31	2.48
Na_2O	3.52	3.87	5.56	4.99	5.11	5.41	5.11	5.51	5.88	5.91	5.87
K_2O	0.70	0.80	5.51	5.61	5.63	5.62	5.39	4.44	4.35	4.85	4.77
P_2O_5	0.28	0.28	0.14	0.11	0.13	0.09	0.15	0.28	0.27	0.18	0.29
Total	103.1	99.3	101.6	101.5	101.5	102.0	101.5	100.6	99.11	99.81	99.73
V	186	179	24	18	20	19	23	57	42	39	42
Cu	52	60	31	47	39	18	26	23	9	22	276
Zn	69	66	64	52	60	53	59	45	34	49	532
Ga	19.8	19.4	24.9	24.6	24.6	23.6	25.1	21.3	20.5	20.4	21.4
Rb	9.5	14.1	223.5	237.4	247.1	249.5	242.8	137.7	123.0	136.2	117.5
Sr	367	360	17	26	15	12	19	373	432	284	316
Y	18.4	17.8	46.7	48.1	50.8	49.6	48.5	29.8	27.5	26.2	26.8
Zr	104	108	956	865	859	852	886	615	553	579	590
Nb	9.5	8.1	109.6	119.1	123.2	122.9	119.4	60.7	56.2	58.0	59.4
Cs	0.15	0.26	11.83	3.81	5.12	13.76	13.60	7.22	5.61	6.58	3.75
Ba	183	237	64	70	49	40	84	667	643	624	619
Sc	23.0	21.5	5.7	4.5	4.5	4.5	5.7	7.6	6.4	6.1	5.5
La	10.7	10.8	64.8	63.5	68.2	69.0	67.9	44.0	41.7	37.2	39.9
Ce	22.6	23.0	120.4	118.0	128.3	128.1	130.9	77.9	72.8	68.8	75.0
Pr	3.06	3.11	12.84	12.40	13.61	13.58	13.38	8.74	8.21	7.47	8.13
Nd	14.7	14.4	44.5	41.9	46.9	45.3	45.5	32.4	30.5	27.5	30.0
Sm	4.01	3.88	8.52	8.03	8.66	8.24	8.50	6.23	5.80	5.29	5.79
Eu	1.36	1.29	0.41	0.38	0.32	0.31	0.34	1.53	1.63	1.31	1.33
Gd	4.09	3.94	7.20	6.71	7.28	7.14	7.13	5.40	5.16	4.64	4.89
Tb	0.67	0.63	1.22	1.23	1.24	1.26	1.32	0.87	0.84	0.76	0.82
Dy	3.83	3.62	7.91	7.69	8.27	8.26	8.25	5.39	5.03	4.72	5.12
Ho	0.72	0.69	1.69	1.68	1.75	1.76	1.77	1.14	1.05	0.99	1.04
Er	1.96	1.88	5.33	5.35	5.79	5.61	5.58	3.37	3.05	3.02	3.11
Tm	0.26	0.26	0.90	0.87	0.97	0.95	0.90	0.55	0.49	0.49	0.49
Yb	1.63	1.67	6.18	6.42	6.86	6.80	6.59	3.75	3.28	3.37	3.47
Lu	0.24	0.23	1.03	1.02	1.10	1.04	1.04	0.58	0.53	0.53	0.53
Hf	2.74	2.77	23.27	22.10	22.34	22.57	23.04	14.65	12.98	13.77	14.16
Ta	0.55	0.47	7.71	8.54	8.72	9.01	8.63	4.47	4.18	4.13	4.34
Pb	2.62	3.08	21.09	23.62	25.11	20.65	21.23	13.50	13.38	14.81	53.73
Th	1.29	1.30	39.66	44.78	47.37	48.20	46.39	25.18	22.18	23.61	24.23
U	0.27	0.33	10.66	11.29	12.16	12.44	11.77	6.18	5.54	6.22	6.02

Supplementary Table 2.1. (cont)

Sample	VRE25	VRE26a	CP1	CP3	CP4	VRE9	MC3	MC5	MC6	VRE27	VRE8
SiO_2	47.99	47.78	44.70	46.91	44.50	49.66	48.07	47.01	48.17	49.93	48.48
TiO_2	1.57	1.40	1.32	1.70	1.27	1.73	1.63	1.52	1.78	1.71	1.48
Al_2O_3	16.80	16.48	14.18	15.05	11.88	17.61	16.06	15.35	16.24	19.03	17.82
FeO_t	11.71	10.89	9.91	10.60	9.58	11.14	11.19	10.80	11.20	11.16	11.17
MnO	0.16	0.17	0.15	0.16	0.13	0.16	0.16	0.16	0.16	0.15	0.16
MgO	6.67	11.26	9.90	9.26	12.23	7.51	8.14	10.20	7.70	6.16	7.37
CaO	9.49	9.94	9.84	11.00	7.16	9.75	9.84	10.29	9.66	9.76	10.84
Na_2O	3.19	2.46	2.55	2.98	2.08	3.37	3.51	3.01	3.53	3.66	3.13
K_2O	0.84	0.97	1.14	1.37	1.11	0.94	0.81	0.93	0.92	0.75	0.81
P_2O_5	0.34	0.43	0.34	0.61	0.28	0.50	0.32	0.40	0.40	0.47	0.44
Total	100.5	102.1	100.1	100.6	99.80	102.3	100.4	100.0	99.53	103.1	102.5
V	203	270	247	269	242	235	231	249	231	237	283
Cu	55	69	61	70	46	47	52	54	40	47	61
Zn	65	60	51	64	46	53	63	55	64	68	54
Ga	19.4	17.8	16.4	19.1	14.6	20.4	19.6	18.4	19.8	21.6	20.1
Rb	19.5	19.4	25.1	27.4	26.0	15.9	15.3	17.8	15.4	11.7	14.4
Sr	502	566	616	980	434	693	627	693	637	590	691
Y	21.6	21.1	20.9	24.4	17.2	26.4	19.6	20.7	22.5	22.2	26.6
Zr	121	126	134	171	124	169	140	142	154	143	136
Nb	11.3	10.0	11.3	21.9	10.1	16.7	12.3	13.6	15.8	11.0	9.9
Cs	0.64	0.85	1.18	0.63	1.62	0.50	0.50	0.79	0.44	0.48	0.53
Ba	238	345	393	643	391	360	328	413	341	309	351
Sc	25.5	35.1	31.2	32.0	29.2	31.9	30.6	32.7	29.8	28.7	37.6
La	13.9	16.6	17.9	30.8	13.7	22.2	15.5	19.6	18.3	14.6	18.1
Ce	28.7	36.0	35.2	55.2	27.9	43.9	33.2	40.3	37.9	31.6	37.2
Pr	3.85	4.64	4.76	7.04	3.72	6.02	4.32	5.28	4.99	4.29	5.21
Nd	18.1	20.9	21.3	31.1	17.1	26.3	19.9	23.1	22.6	19.9	23.4
Sm	4.58	4.93	4.99	6.68	3.96	6.32	4.69	5.28	5.31	5.09	5.80
Eu	1.57	1.50	1.50	2.10	1.26	2.05	1.55	1.71	1.85	1.73	1.91
Gd	4.74	4.62	4.77	6.37	3.77	6.15	4.51	5.00	5.25	4.94	5.99
Tb	0.79	0.70	0.76	0.92	0.63	0.96	0.76	0.77	0.81	1.46	0.86
Dy	4.33	4.14	4.15	5.11	3.43	5.50	4.02	4.09	4.55	4.47	5.43
Ho	0.84	0.81	0.79	0.95	0.65	1.06	0.79	0.78	0.90	0.88	1.08
Er	2.32	2.25	2.14	2.50	1.82	2.84	2.14	2.19	2.35	2.34	2.93
Tm	0.32	0.32	0.31	0.34	0.25	0.39	0.30	0.29	0.32	0.32	0.41
Yb	2.01	1.96	1.94	2.20	1.63	2.40	1.96	1.84	2.08	2.07	2.65
Lu	0.29	0.30	0.30	0.30	0.23	0.35	0.28	0.27	0.30	0.30	0.37
Hf	3.09	3.26	3.41	4.30	3.19	4.37	3.63	3.63	4.04	3.66	3.82
Ta	0.65	0.58	0.69	1.28	0.60	0.97	0.72	0.79	0.94	0.61	0.57
Pb	3.77	4.21	5.71	8.31	4.13	4.47	4.06	4.92	4.17	3.62	6.24
Th	1.55	3.14	3.43	6.68	3.01	3.17	2.50	3.56	2.64	1.67	2.94
U	0.29	0.78	0.98	1.38	0.69	0.62	0.66	0.92	0.59	0.48	0.66

Supplementary Table 2.1. (cont)

Sample	VRE11	VRE42	VRE43	VRE44	VRE45	VRE1	VRE4	VRE6	VRE16a	VRE16b	VRE17
SiO_2	47.23	49.45	48.21	45.69	45.96	56.32	54.21	54.09	68.93	66.57	56.74
TiO_2	1.49	1.58	1.75	1.56	1.70	1.00	1.05	1.03	0.50	0.54	1.07
Al_2O_3	16.07	17.64	17.98	14.85	16.06	18.79	18.04	17.72	15.87	16.59	19.42
FeO_t	10.91	11.07	9.91	10.76	11.83	8.17	8.23	7.85	2.32	2.66	8.42
MnO	0.16	0.15	0.15	0.16	0.17	0.13	0.13	0.12	0.07	0.08	0.13
MgO	8.81	7.11	7.74	9.49	8.45	4.55	5.49	5.74	0.10	0.65	4.93
CaO	10.67	9.45	10.27	10.89	10.50	7.58	7.80	7.78	1.50	2.10	7.84
Na_2O	3.28	3.17	3.84	3.33	3.10	3.68	3.49	3.25	4.39	4.74	3.87
K_2O	1.18	0.84	1.29	1.01	0.88	1.60	1.48	1.48	4.51	4.19	1.56
P_2O_5	0.47	0.36	0.59	0.47	0.39	0.36	0.38	0.37	0.12	0.13	0.31
Total	102.0	100.7	101.5	100.2	98.89	102.6	100.7	100.3	101.1	103.1	103.9
V	265	234	259	243	265	205	212	215	32	43	206
Cu	58	43	55	80	107	71	49	50	31	49	38
Zn	53	65	57	69	73	59	53	46	46	50	55
Ga	19.1	20.5	20.2	18.1	19.6	19.9	19.6	19.2	16.5	16.9	18.9
Rb	23.4	14.8	29.8	19.4	15.9	35.5	31.3	33.5	158.7	138.6	47.1
Sr	807	568	897	724	619	929	842	851	147	184	499
Y	24.8	24.2	29.3	22.8	24.3	22.1	21.5	22.4	42.5	42.5	22.4
Zr	147	131	202	153	140	153	164	167	478	449	168
Nb	14.8	9.6	21.8	15.8	13.6	6.7	8.1	7.9	15.1	14.5	7.9
Cs	0.86	0.24	1.02	0.68	0.41	2.32	1.16	1.28	6.34	3.42	0.72
Ba	502	333	529	405	307	472	434	472	782	785	363
Sc	33.2	30.3	32.6	31.5	33.2	25.2	28.2	29.1	9.3	10.4	26.7
La	26.0	16.3	28.9	23.8	17.0	25.7	25.0	25.8	43.7	43.0	21.9
Ce	48.5	31.9	56.8	45.2	34.5	50.8	50.9	51.4	87.2	85.4	44.7
Pr	6.33	4.54	7.52	6.01	4.75	6.64	6.74	6.76	10.94	10.79	5.79
Nd	26.8	21.1	32.8	26.5	22.1	27.5	27.4	27.8	44.2	43.3	24.8
Sm	6.04	5.37	7.30	5.75	5.48	6.00	6.02	6.15	9.02	8.97	5.28
Eu	1.96	1.79	2.26	1.79	1.80	1.63	1.67	1.66	1.51	1.64	1.44
Gd	5.79	5.53	7.03	5.72	5.42	5.01	5.17	5.08	7.96	7.84	4.75
Tb	0.87	0.89	1.12	0.86	0.87	0.75	0.76	0.78	1.23	1.24	0.77
Dy	5.07	5.00	5.84	4.78	4.85	4.31	4.23	4.45	7.53	7.58	4.31
Ho	0.99	0.97	1.14	0.91	0.96	0.84	0.86	0.90	1.56	1.57	0.88
Er	2.61	2.50	3.12	2.43	2.54	2.38	2.32	2.37	4.61	4.50	2.48
Tm	0.37	0.33	0.41	0.31	0.35	0.35	0.34	0.36	0.71	0.70	0.34
Yb	2.30	2.25	2.73	2.07	2.14	2.33	2.32	2.33	4.72	4.67	2.41
Lu	0.32	0.32	0.40	0.30	0.32	0.34	0.33	0.35	0.70	0.70	0.34
Hf	3.92	3.63	4.94	4.01	3.64	4.40	4.41	4.58	13.05	12.35	4.49
Ta	0.82	0.57	1.26	0.94	0.81	0.40	0.47	0.48	1.12	1.11	0.55
Pb	6.11	4.16	5.65	6.15	6.06	17.90	10.97	198.44	21.59	18.19	7.95
Th	5.18	2.29	3.95	3.82	2.04	8.81	5.97	6.63	22.69	22.13	6.67
U	1.17	0.36	0.87	0.85	0.49	2.26	1.25	1.36	4.97	4.71	1.70

Supplementary Table 2.1. (cont)

Duplicates of 10% HCl leached samples

Sample	Ga	Rb	Sr	Y	Zr	Nb	Hf	Pb
	ppm	ppm	ppm	ppm	ppm	ppm	ppm	ppm
SM16	18.8	20.4	802.0	27.5	188.2	25.7	4.2	3.4
VRE21	19.9	24.8	631.6	28.9	173.3	20.3	4.0	3.7
VRE46a	20.2	14.5	566.8	23.0	119.1	12.4	3.2	3.4
VRE43	20.3	30.3	808.3	27.7	166.7	18.5	3.0	5.9
CP4	12.7	32.4	486.7	19.1	107.8	9.0	4.2	4.2
VRE27	19.1	14.9	580.4	27.0	129.5	9.8	3.1	6.5
VRE11	19.0	25.1	726.9	24.1	124.2	12.4	2.9	7.4
VRE27R	18.8	15.0	575.4	27.1	129.2	9.5	4.1	6.2
BCR-2	21.6	49.3	342.5	37.2	184.3	12.6	4.7	12.5
BCR-2 recommended value	23±2	48±2	346±14	37±2	188±16	12.6±0.4	4.8±0.2	11±2

Trace-element analysis performed by XRF at the School of Earth and Environmental Sciences, University of Wollongong, Wollongong, Australia

Supplementary Table 2.2. Reproducibility of LA-ICP-MS data for BCR-2 rock standard.

All values are in ppm

Standard: BCR-2	^{45}Sc	^{51}V	^{65}Cu	^{66}Zn	^{71}Ga	^{85}Rb	^{88}Sr	^{89}Y	^{91}Zr	^{93}Nb	^{133}Cs	^{137}Ba	^{139}La	^{140}Ce	^{141}Pr	^{146}Nd
BCR-2	37.0	427	20	109	22.4	46.5	349	35.2	190	13.0	1.14	695	26.2	52.9	6.85	29.4
BCR-2	38.2	424	20	105	22.0	46.6	358	36.1	197	13.3	1.15	706	26.8	52.9	6.97	29.7
BCR-2	35.5	425	19	117	21.5	45.0	334	33.8	181	12.3	1.14	664	24.8	50.3	6.48	28.0
BCR-2	36.1	424	21	116	21.9	45.5	339	34.4	186	12.4	1.15	663	25.5	50.9	6.61	28.2
BCR-2	37.0	426	21	113	22.0	46.0	340	34.6	189	12.5	1.13	678	25.4	51.1	6.56	28.5
BCR-2	34.5	416	19	114	21.5	43.3	312	30.7	176	11.6	1.06	625	22.6	46.4	5.96	25.8
BCR-2	36.1	434	19	114	22.0	47.0	343	34.4	185	12.5	1.14	676	25.0	51.7	6.62	28.3
BCR-2	35.6	441	19	118	22.7	48.2	346	33.6	182	12.5	1.20	685	24.9	52.7	6.64	28.3
BCR-2	36.7	431	20	125	22.0	46.7	346	34.9	187	12.7	1.15	683	25.8	51.8	6.69	28.7
BCR-2	35.2	426	19	116	21.7	45.5	334	33.4	182	12.3	1.12	665	24.6	50.6	6.44	27.8
BCR-2	35.3	438	21	122	22.4	47.0	334	32.9	183	12.4	1.13	667	24.4	51.2	6.46	27.5
BCR-2	35.0	431	20	118	21.7	46.7	332	32.9	180	12.2	1.11	665	24.5	50.9	6.40	27.4
Average	36.0	429	20	116	22.0	46.2	339	33.9	185	12.5	1.14	673	25.0	51.1	6.56	28.1
Std dev	1.0	6.7	0.7	5.3	0.4	1.2	11.3	1.4	5.32	0.4	0.03	20.1	1.1	1.7	0.25	1.0
Std dev relative %	2.9	1.6	3.7	4.6	1.6	2.7	3.3	4.1	2.88	3.3	2.92	3.0	4.2	3.4	3.85	3.5
Reference value (certificate)	33±2	416±14	19±2	127±9	23±2	48±2	346±14	37±2	188±16		1.1±0.1	683±28	25±1	53±2	6.8±0.3	28±2
Difference in ppm (reference-average)	3.00	12.58	0.83	11.37	1.00	1.83	7.06	3.10	3.09		0.04	10.23	0.04	1.89	0.24	0.13
Error % to recommended value	9.09	3.02	4.39	8.95	4.34	3.82	2.04	8.38	1.64		3.22	1.50	0.14	3.57	3.57	0.48

Supplementary Table 2.2. (cont)

^{147}Sm	^{153}Eu	^{157}Gd	^{159}Tb	^{163}Dy	^{165}Ho	^{166}Er	^{169}Tm	^{172}Yb	^{175}Lu	^{178}Hf	^{181}Ta	^{205}Tl	^{208}Pb	^{232}Th	^{238}U
6.94	2.04	6.76	1.07	6.64	1.35	3.84	0.53	3.64	0.52	5.24	0.80	0.26	10.62	6.33	1.66
6.98	2.09	6.98	1.09	6.86	1.40	4.00	0.55	3.80	0.53	5.47	0.81	0.24	10.40	6.44	1.66
6.62	1.95	6.48	1.03	6.26	1.29	3.63	0.51	3.48	0.51	4.97	0.77	0.26	10.58	6.01	1.65
6.69	1.97	6.59	1.02	6.36	1.30	3.67	0.52	3.44	0.50	5.05	0.77	0.24	10.76	6.01	1.63
6.83	1.95	6.68	1.02	6.54	1.33	3.70	0.52	3.61	0.51	5.10	0.78	0.25	10.61	6.12	1.65
6.13	1.77	5.97	0.92	5.76	1.17	3.29	0.47	3.14	0.46	4.51	0.70	0.21	10.12	5.43	1.53
6.90	1.98	6.61	1.03	6.33	1.31	3.64	0.51	3.51	0.49	4.97	0.77	0.25	10.87	6.00	1.70
6.58	1.97	6.51	1.01	6.34	1.29	3.59	0.50	3.46	0.50	4.89	0.75	0.24	11.14	5.94	1.74
6.82	2.01	6.78	1.05	6.51	1.33	3.76	0.52	3.51	0.52	5.03	0.79	0.24	11.17	6.19	1.69
6.45	1.92	6.42	1.01	6.26	1.26	3.58	0.51	3.44	0.49	4.87	0.76	0.24	10.59	5.94	1.63
6.40	1.96	6.37	1.01	6.28	1.27	3.58	0.50	3.43	0.49	4.80	0.74	0.25	11.14	5.89	1.65
6.39	1.95	6.35	1.00	6.22	1.27	3.61	0.51	3.35	0.49	4.70	0.76	0.25	10.72	5.92	1.64
6.64	1.96	6.54	1.02	6.36	1.30	3.66	0.51	3.48	0.50	4.97	0.77	0.24	10.73	6.02	1.65
0.26	0.08	0.26	0.04	0.27	0.06	0.17	0.02	0.16	0.02	0.25	0.03	0.01	0.32	0.25	0.05
3.99	3.89	3.94	4.11	4.22	4.27	4.66	3.81	4.64	3.63	5.02	3.73	5.68	2.95	4.19	2.94
6.7±0.3	2.0±0.2	6.8±0.3	1.07±0.04		1.33±0.06		0.54	3.5±0.2	0.51±0.02	4.8±0.2			11±2	6.2±0.7	1.69±0.19
0.06	0.04	0.21	0.05		0.03		0.03	0.02	0.01	0.17			0.27	0.18	0.04
0.85	1.80	3.09	4.60		2.47		5.01	0.45	2.23	3.48			2.48	2.94	2.25